OSPL
Organic Semiconductor Process Lab.

KOREA UNIVERSITY

Electrochemical conversion of CO_2 using single atom decorated catalysts

Soo Young Kim[a]

[a] Department of Materials Science and Engineering, Korea University

Soo Young Kim's research

OSPL
Organic Semiconductor Process Lab.

2D Materials MOF

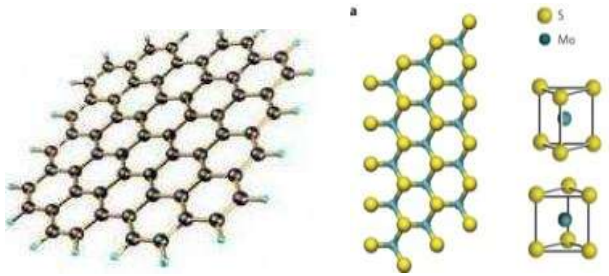

Science **328**, 1373 (2010)
Adv. Func. Mater. **22**, 4724 (2012)
ACS Nano **9**, 4146 (2015)
Adv. Func. Mater. **25**, 4512 (2015)
Sci. Adv. **4**, eaas8721 (2018)
Sci. Adv. **6**, eabb5898 (2020)

OLED Perov LED

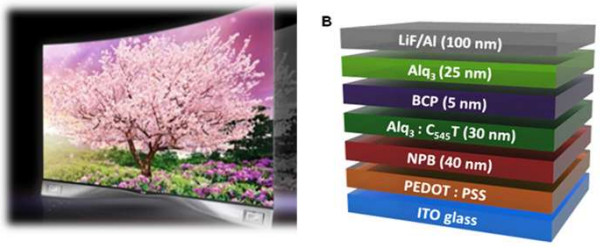

Adv. Mater. **29**, 1702598 (2017)
Adv. Func. Mater. **28**, 1705783 (2018)
Adv. Mater. **30**, 174002 (2018)
Nano Energy **70**, 104497 (2020)
Adv. Func. Mater. **31**, 2102770 (2021)
ACS Photonics **8**, 1979 (2021)
Adv. Mater. ***36***, 2309531 (2024)

Solar cells Photodetector Electrochromic

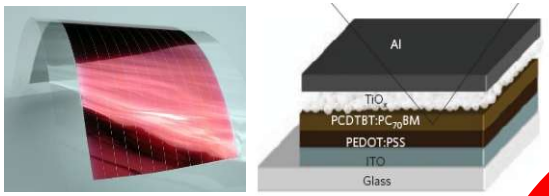

Adv. Func. Mater. **26**, 4213 (2016)
ACS AMI **10**, 43785 (2018)
Mater. Today Advances **14**, 100232 (2022
Solar RRL **6**, 2200485 (2022)
Small Methods **8**, 2300207 (2024)
Adv. Sci. ***11***, 2406657 (2024)

Gas sensors & Water splitting & CO2 reduction

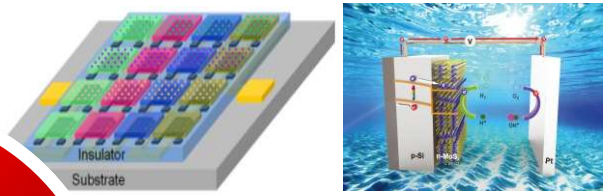

Energy & Environ. Sci. **9**, 2240 (20
ACS Catalysis **10**, 420 (2020)
Applied Catalysis B **270**, 118895 (2020)
Adv. Mater. **35**, 2208224 (2023)
J. Mater. Chem. A **12**, 11090 (2024)
ACS Nano **19**, 18698 (2025)

Ubiquitous Energy Harvesting

Soo Young Kim's research

OSPL
Organic Semiconductor Process Lab.

2D Materials MOF

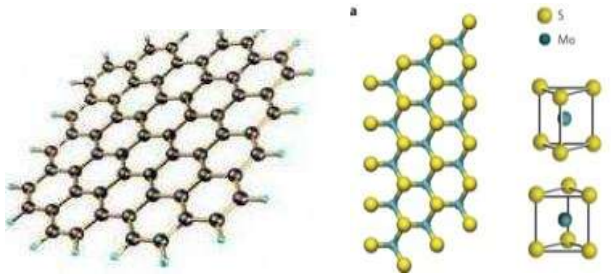

Science **328**, 1373 (2010)
Adv. Func. Mater. **22**, 4724 (2012)
ACS Nano **9**, 4146 (2015)
Adv. Func. Mater. **25**, 4512 (2015)
Sci. Adv. **4**, eaas8721 (2018)
Sci. Adv. **6**, eabb5898 (2020)

OLED Perov LED

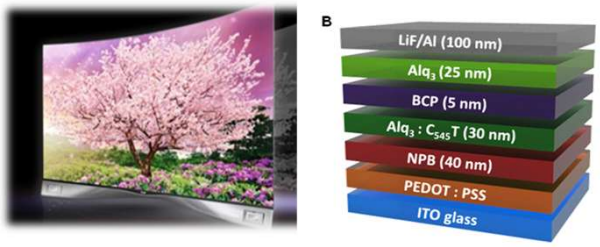

Adv. Mater. **29**, 1702598 (2017)
Adv. Func. Mater. **28**, 1705783 (2018)
Adv. Mater. **30**, 174002 (2018)
Nano Energy **70**, 104497 (2020)
Adv. Func. Mater. **31**, 2102770 (2021)
ACS Photonics **8**, 1979 (2021)
Adv. Mater. **36**, 2309531 (2024)

Solar cells Photodetector Electrochromic

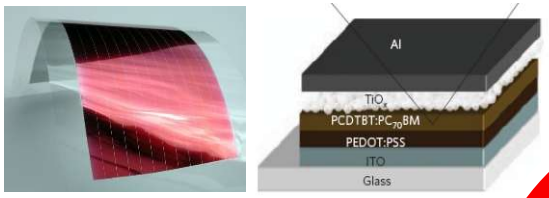

Adv. Func. Mater. **26**, 4213 (2016)
ACS AMI **10**, 43785 (2018)
Mater. Today Advances **14**, 100232 (2022
Solar RRL **6**, 2200485 (2022)
Small Methods **8**, 2300207 (2024)
Adv. Sci. ***11***, 2406657 (2024)

Gas sensors & Water splitting & CO2 reduction

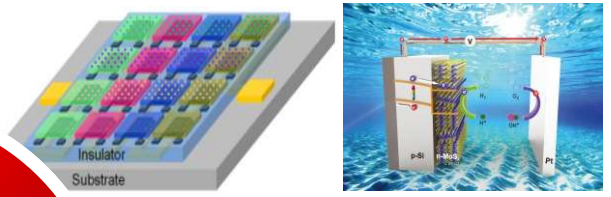

Energy & Environ. Sci. **9**, 2240 (20
ACS Catalysis **10**, 420 (2020)
Applied Catalysis B **270**, 118895 (2020)
Adv. Mater. **35**, 2208224 (2023)
J. Mater. Chem. A **12**, 11090 (2024)
ACS Nano **19**, 18698 (2025)

Ubiqu tous Energy Harvesting

Energy consumption and concern

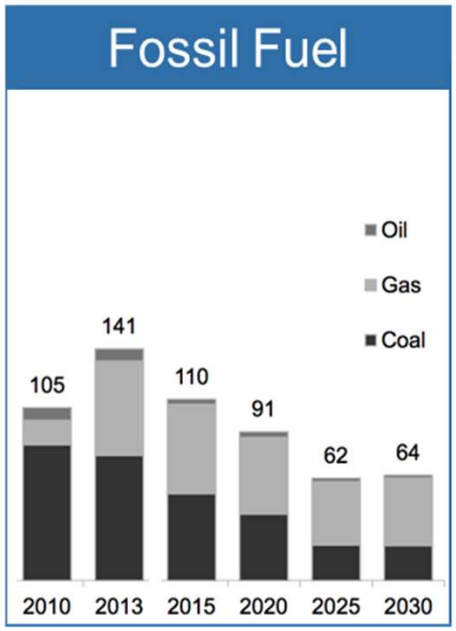

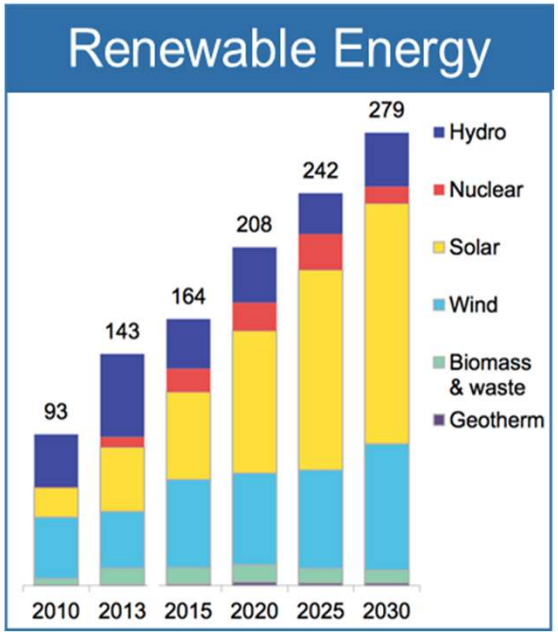

CO_2 removal strategies

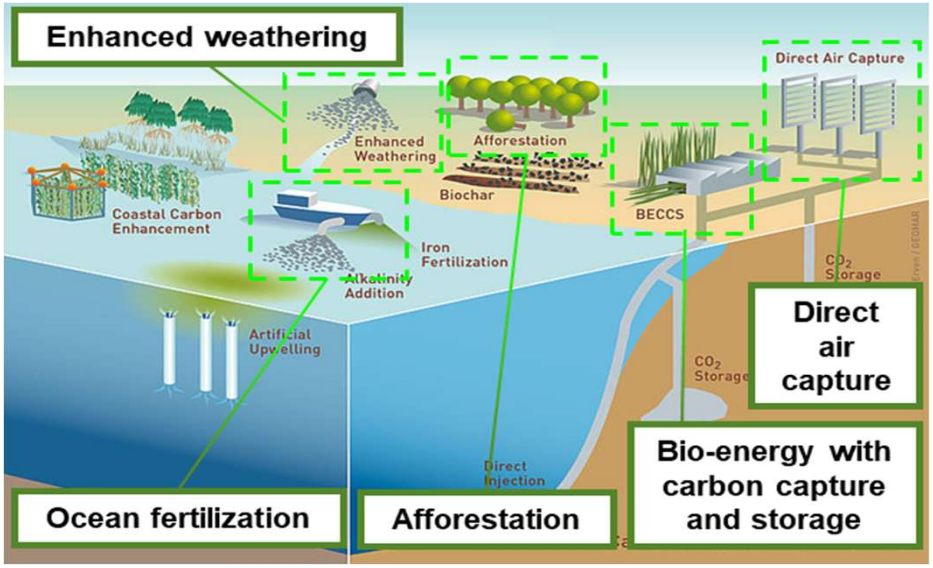

CO_2 electrochemical reaction

OSPL
Organic Semiconductor Process Lab.

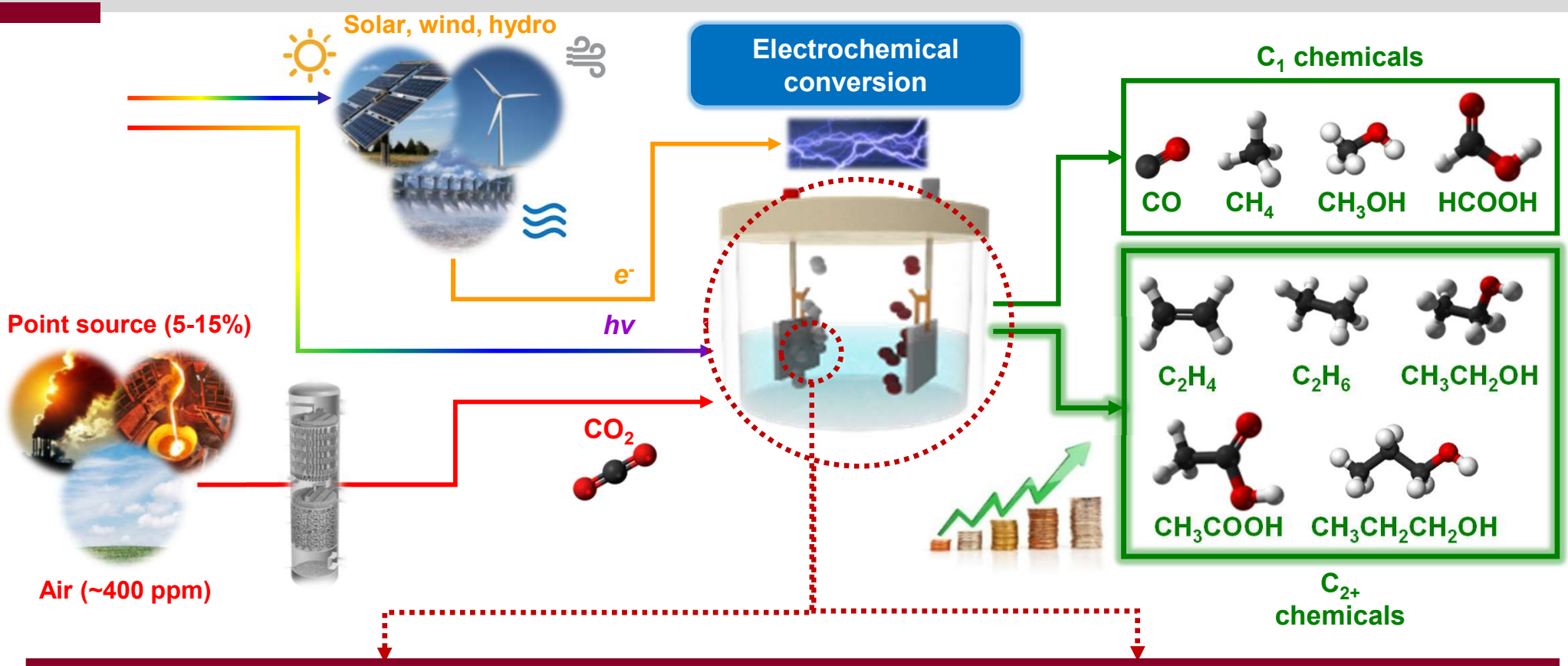

Development of high performance electrocatalyst

Composition engineering | Structure engineering | Substrate engineering | Dimensionality | Pore & surface area

Electrocatalysts

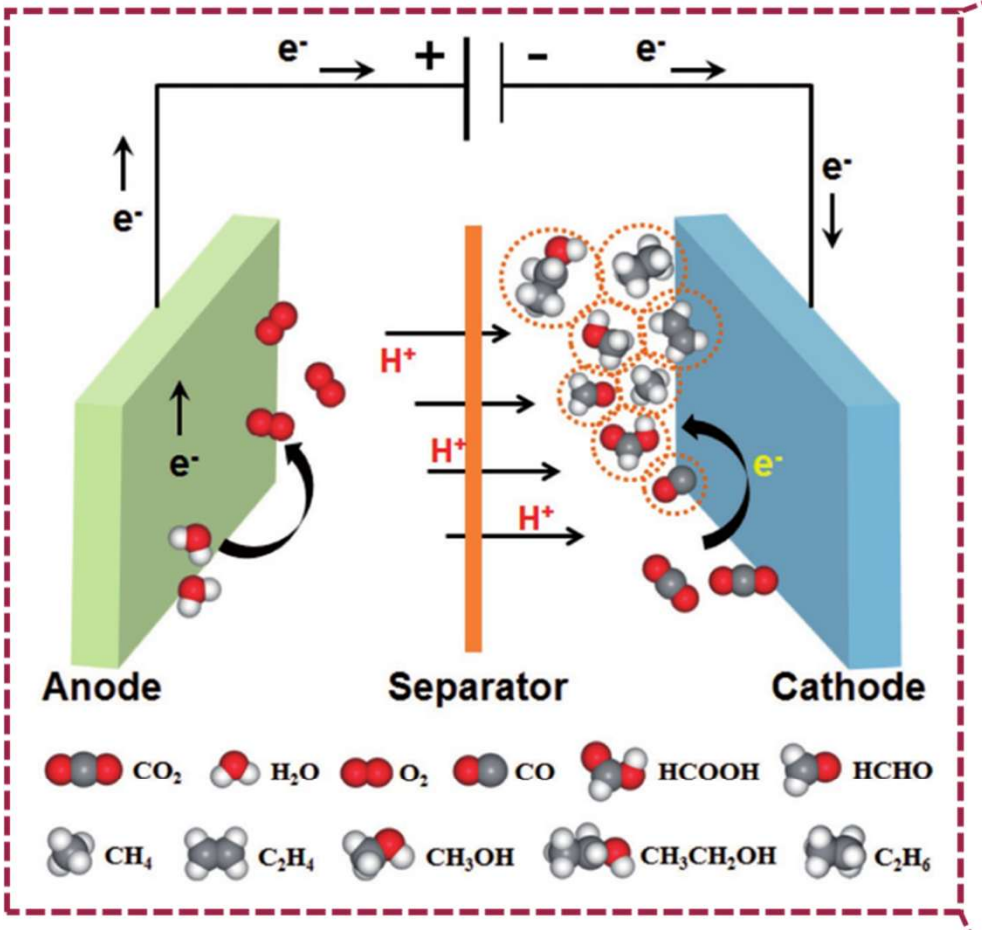

Advanced Science 5 (2018): 1700275.

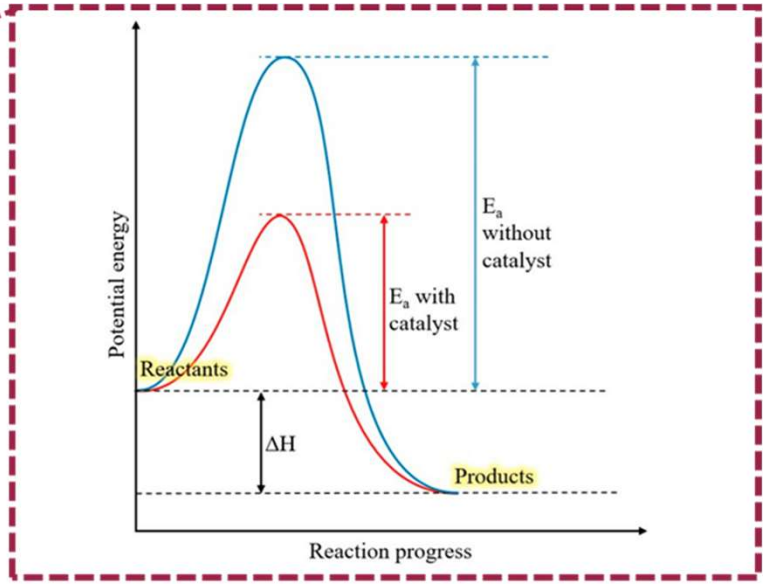

Catalysts 10.11 (2020): 1260.

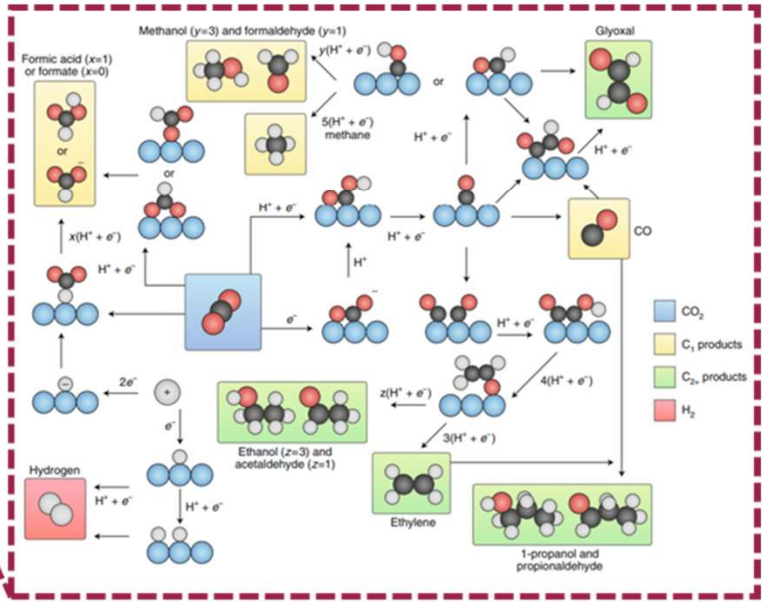

Environmental Chemistry Letters 19 (2021): 941–967.

Why **electrocatalysts**?

- can reduce activation energy(E_a)
- can control the **selectivity** of products

Metal Organic Frameworks (MOFs)

MOFs ?

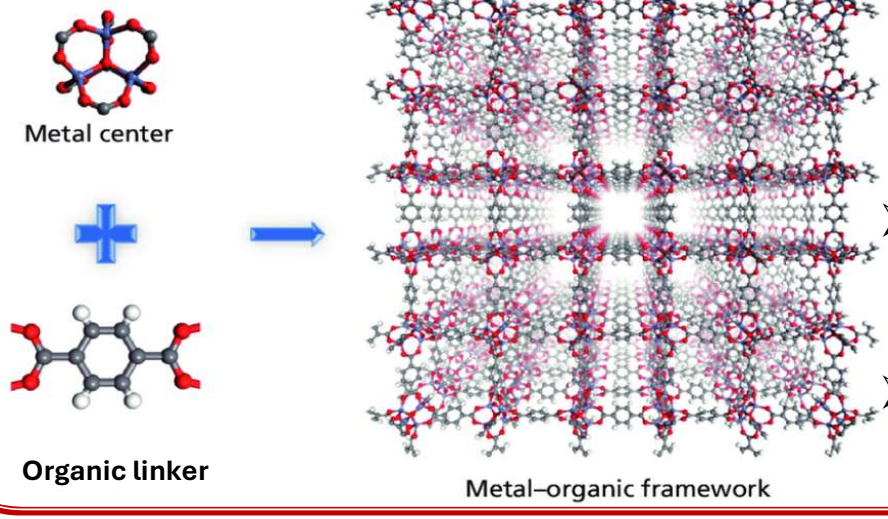

- Metal-organic frameworks are a class of compounds consisting of metal ions or clusters coordinated to organic ligands.
- Advantages : Pore size selectivity, High surface area, easy synthetic process
- Application : Sensing, LIB, supercapacitor, HER, (photo, electrochemical) CO_2RR

MOFs candidate for eCO_2RR

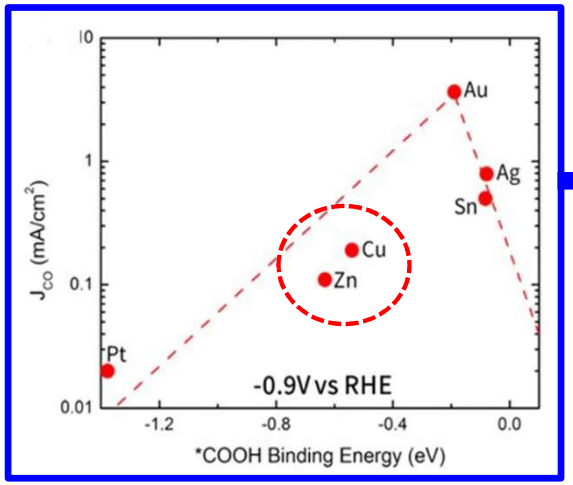

Volcano plot

CO_2 absorption

CO desorption

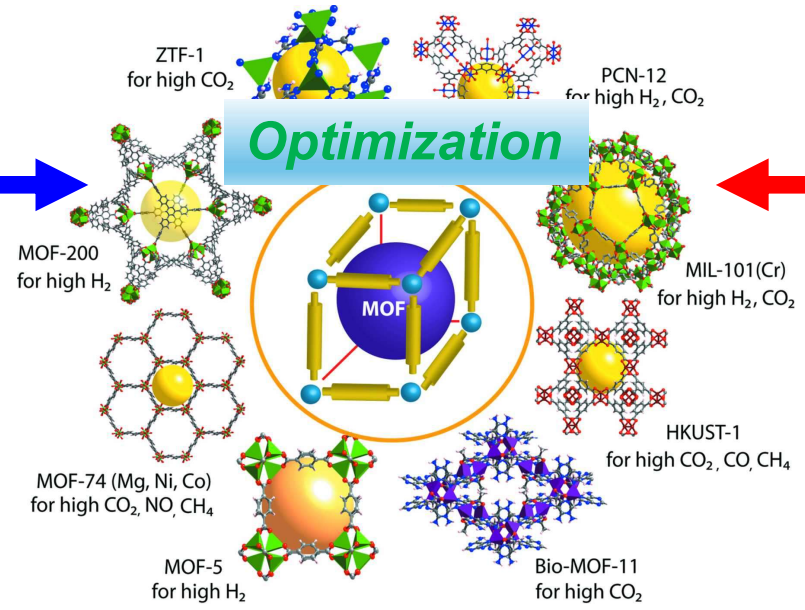

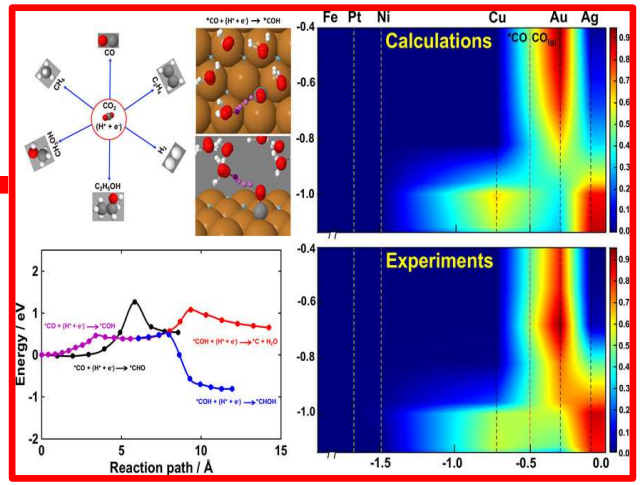

Density Functional Theory

Experimental Methods

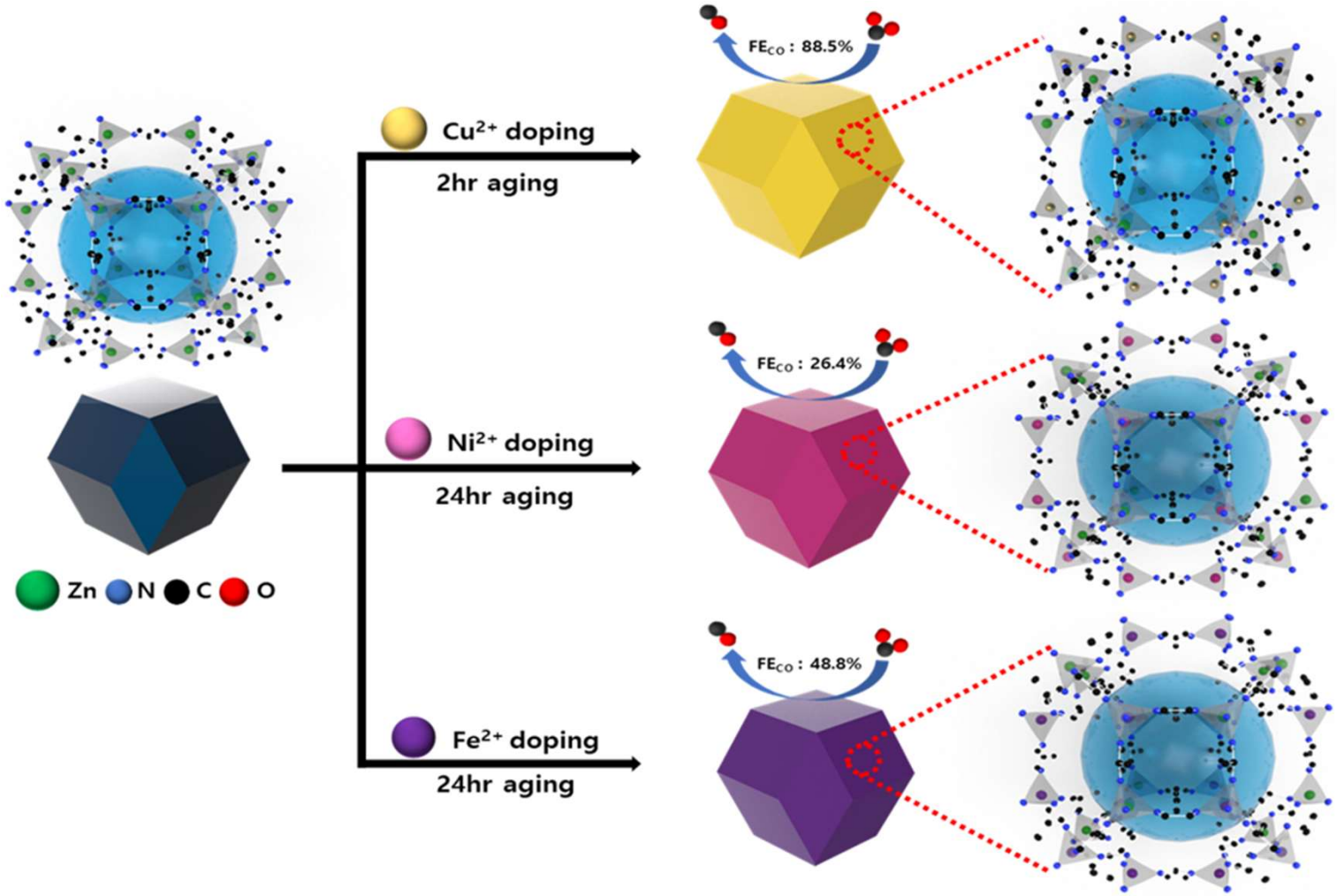

- Doping various transition metal ions into ZIF-8 *via* facile one step process.

'M_xZn_y/ZIF-8'

M: transition metal ions
x:y : molar ratio (0.1:0.9, 0.3:0.7, 0.5:0.5)

Characterizations

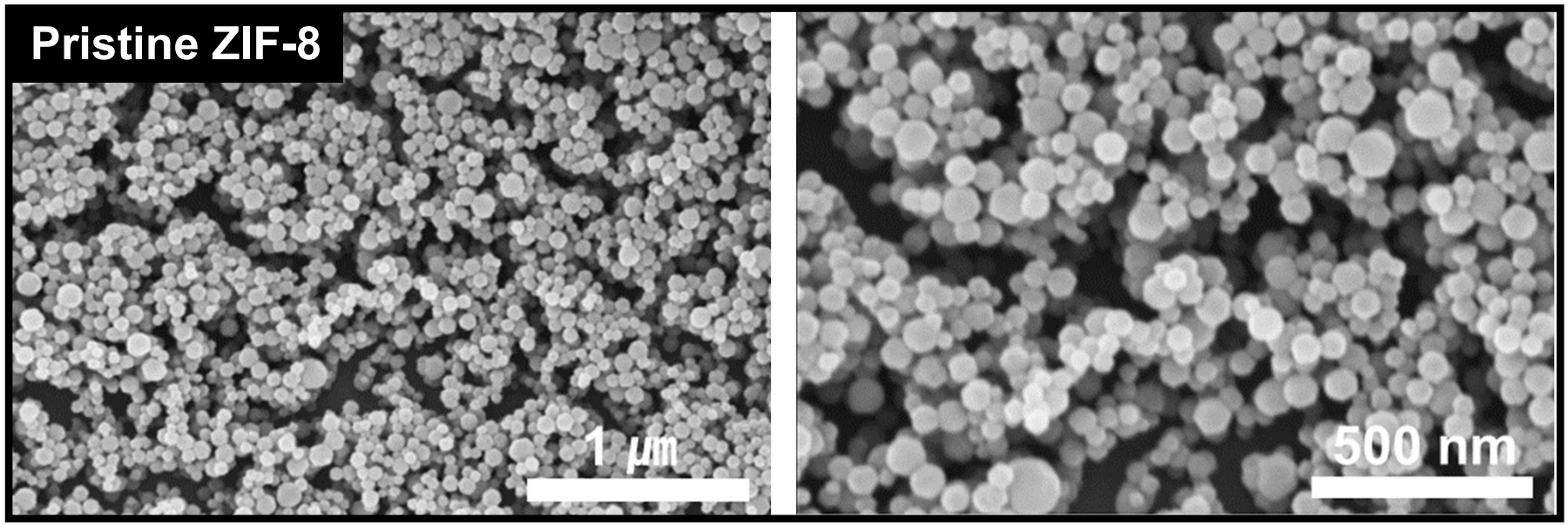

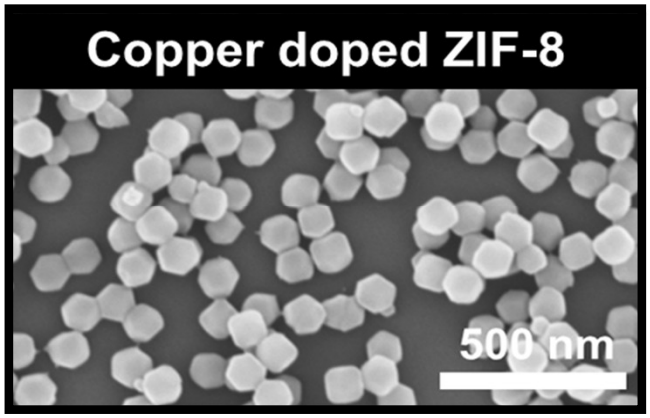

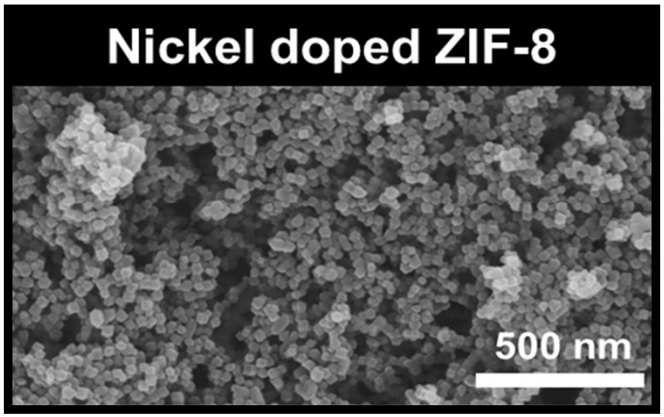

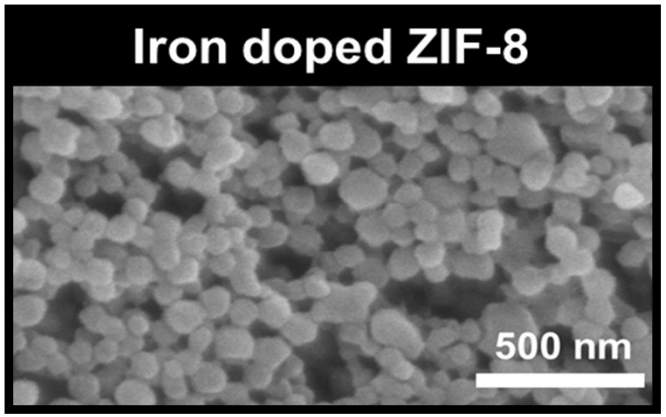

From SEM images,

- ZIF-8 and Cu_xZn_y/ZIF-8 exhibit a rhombic dodecahedron structure with a particle size of 80-100 nm.
- Ni_xZn_y/ZIF-8 and Fe_xZn_y/ZIF-8 reveal a uniform diameter of ~30 nm and ~50 nm, respectively.

Electrochemical performance

CO and H_2 Faradaic efficiencies of a) $Ni_{0.1}Zn_{0.9}$/ZIF-8, b) $Ni_{0.3}Zn_{0.7}$/ZIF-8, c) $Ni_{0.5}Zn_{0.5}$/ZIF-8, d) $Fe_{0.1}Zn_{0.9}$/ZIF-8, e) $Fe_{0.3}Zn_{0.7}$/ZIF-8, f) $Fe_{0.5}Zn_{0.5}$/ZIF-8, g) $Cu_{0.1}Zn_{0.9}$/ZIF-8, h) $Cu_{0.3}Zn_{0.7}$/ZIF-8, and i) $Cu_{0.5}Zn_{0.5}$/ZIF-8

Ni_xZn_y /ZIF-8

Fe_xZn_y/ZIF-8

Cu_xZn_y/ZIF-8

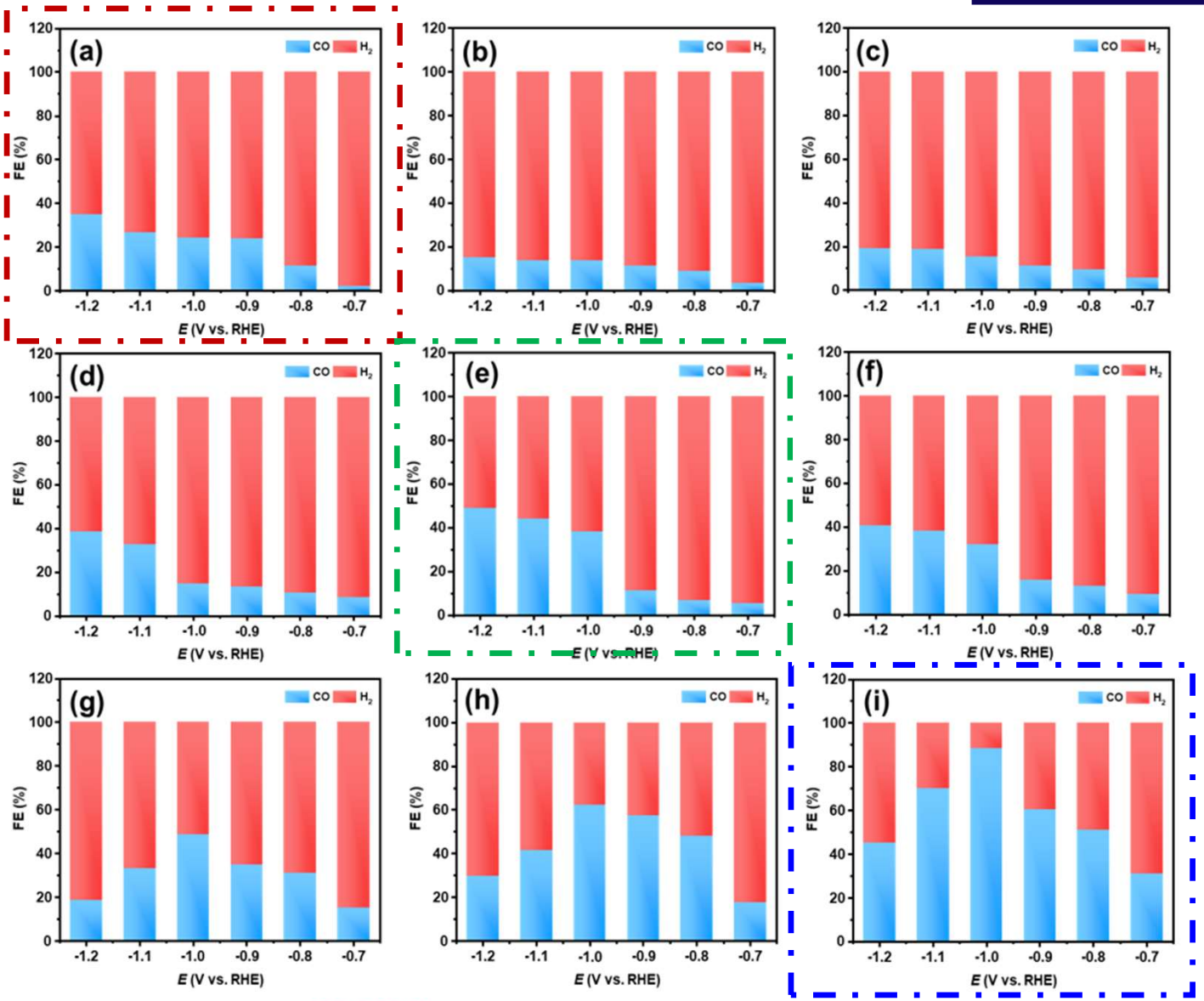

Competitive reaction

Characterizations

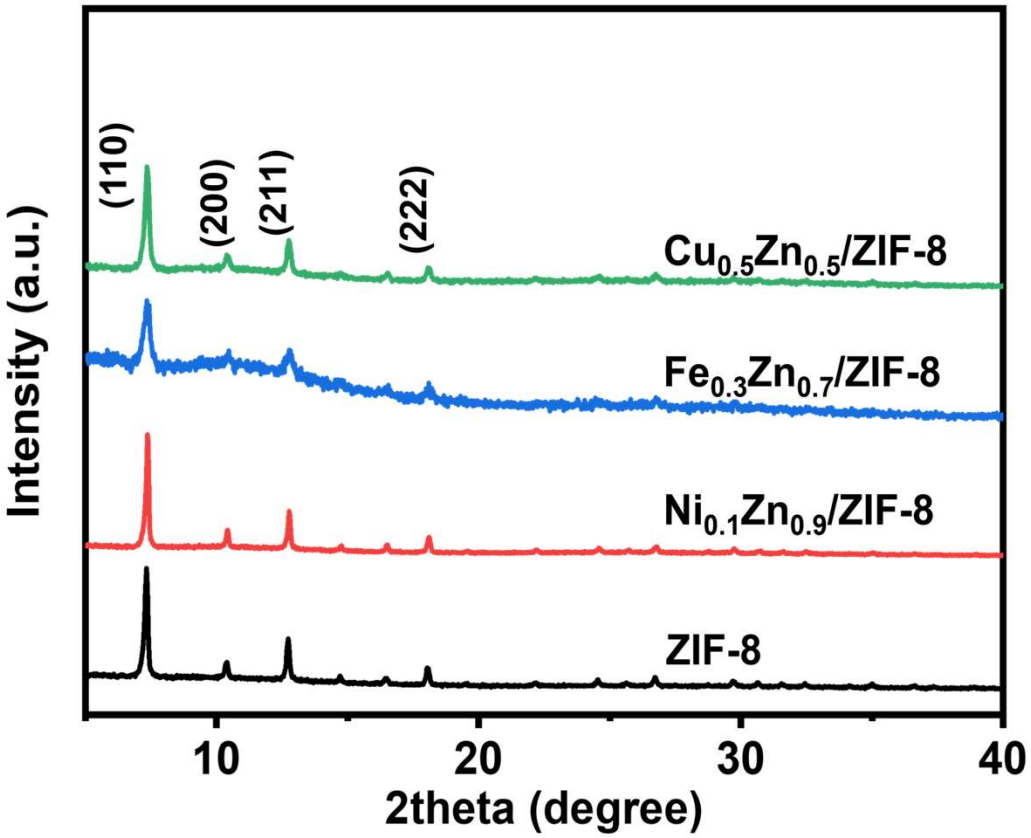

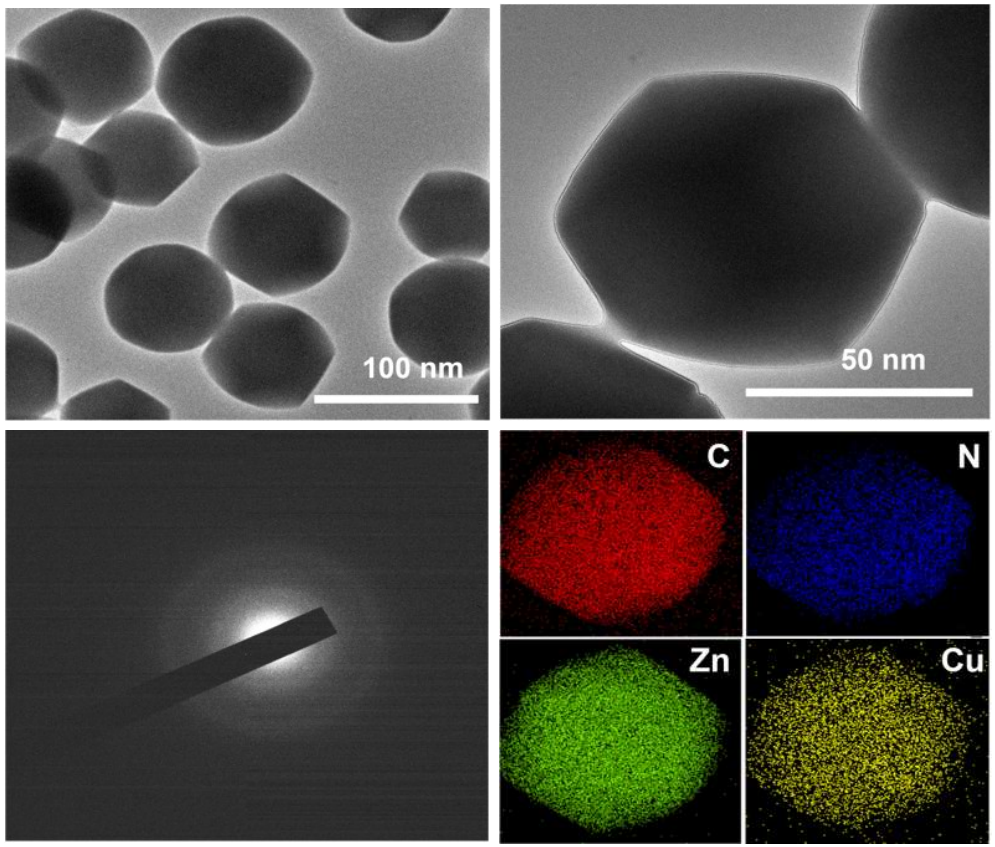

- The intensive XRD peaks of M_xZn_y/ZIF-8 are assigned to (110), (200), (211), and (222) planes; negligible peak change after doping with transition metal ions.
- $Cu_{0.5}Zn_{0.5}$/ZIF-8 characterizes the hexagonal facets.
- EDS indicates that Cu, Zn, N and C are homogeneously distributed on the ZIF-8 structure.

Characterizations

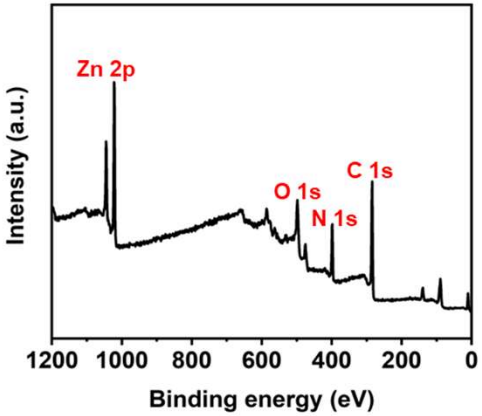

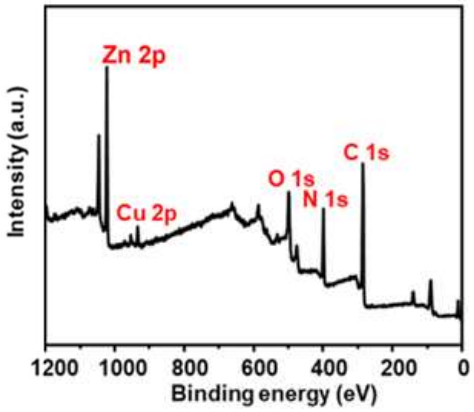

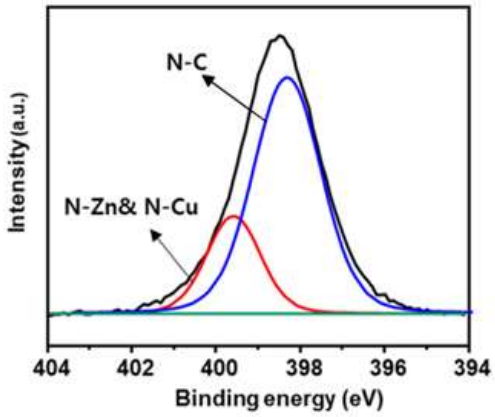

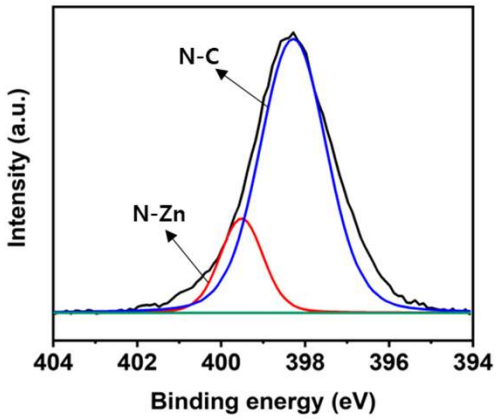

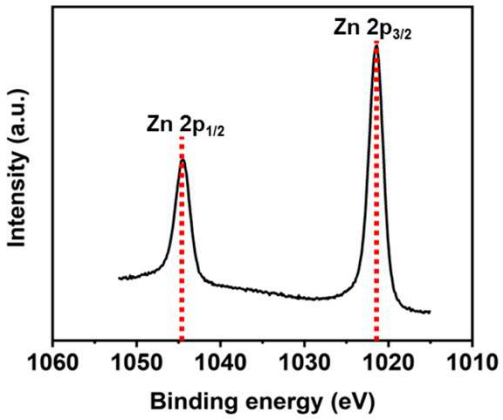

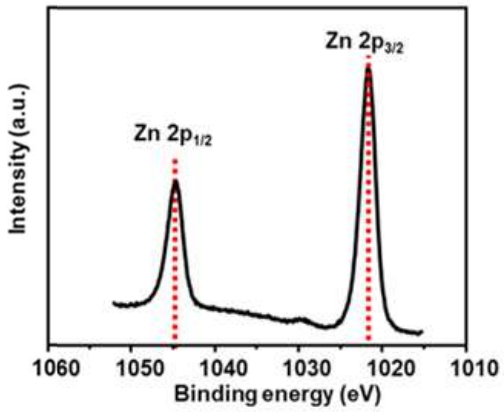

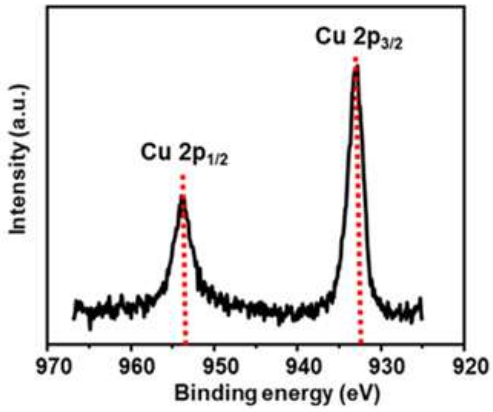

- From the N 1s region, N-Zn and N-C peak are assigned to 399.3 and 398 eV.
- Zn $2p_{1/2}$ and Zn $2p_{3/2}$ peaks are assigned to 1044.7 and 1021.6 eV. → Zn^{2+} valence state
- The deconvoluted N 1s spectrum confirms the chemical coordination of Cu and Zn with N, attributed to 399.3 eV peak, and the formation of N–C bond at 397.9 eV.
- It reveals existence of single electronic state of Cu^{2+} and Zn^{2+} in $Cu_{0.5}Zn_{0.5}$/ZIF-8.

Characterizations

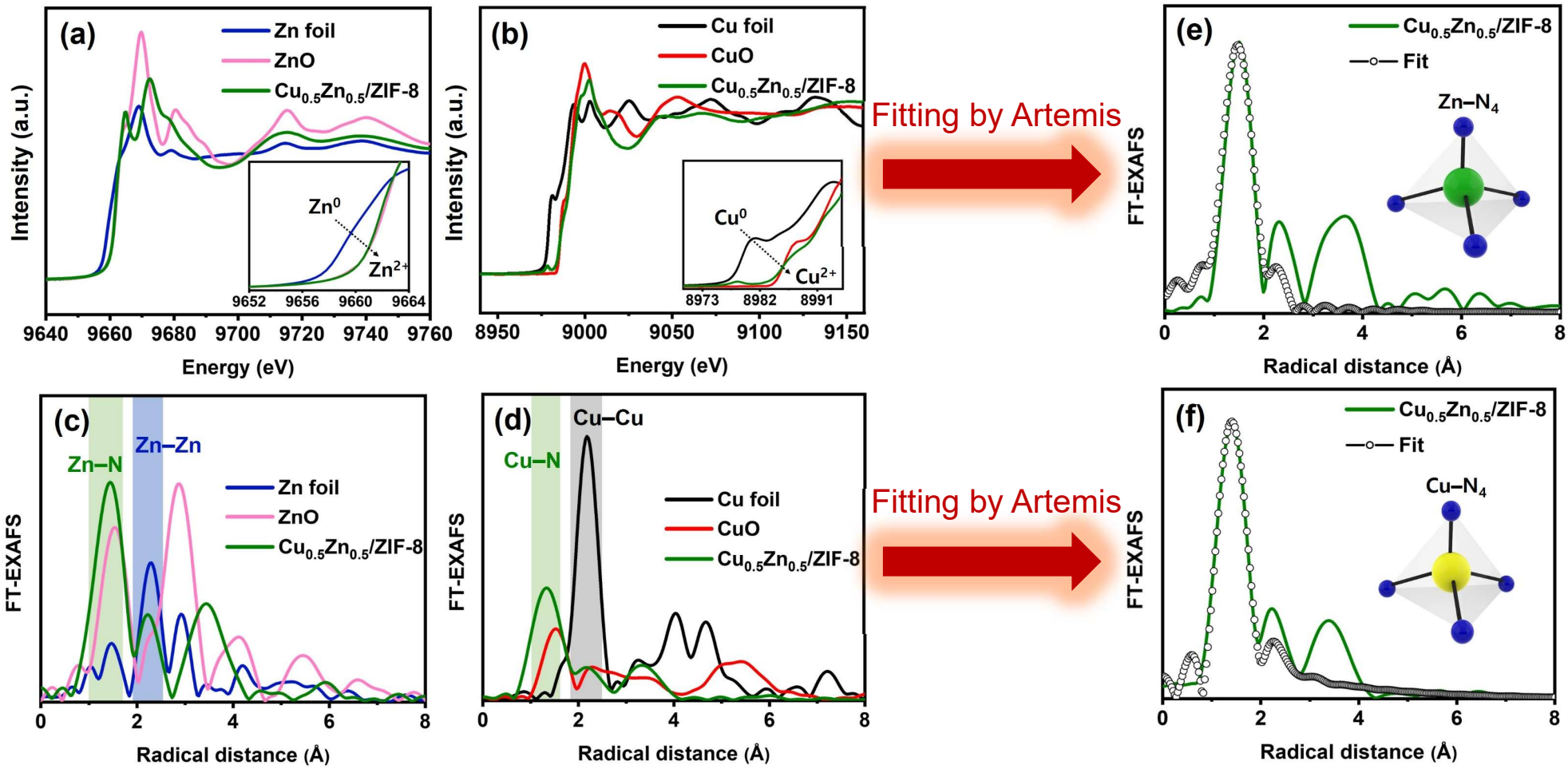

- From Zn K-edge and Cu K-edge of XANES spectra, valence states of Zn and Cu atoms are Zn^{2+} and Cu^{2+}.
- From Zn K-edge and Cu K-edge of EXAFS spectra, Zn-N and Cu-N coordination are dominant.
- EXAFS fitting - coordination number : $Zn\text{-}N_4$ (4), $Cu\text{-}N_4$ (3.97)

Electrochemical performance

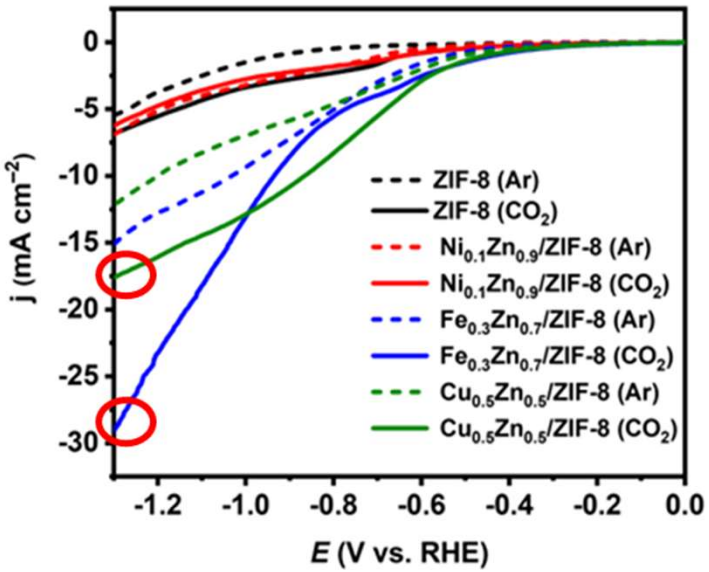

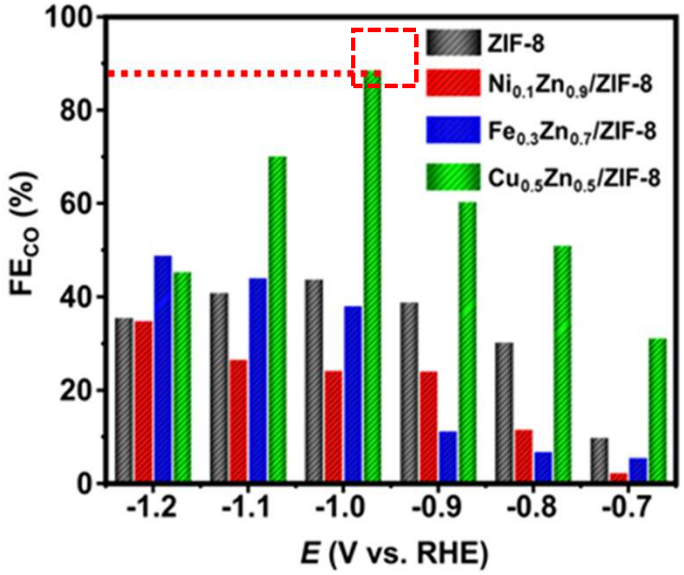

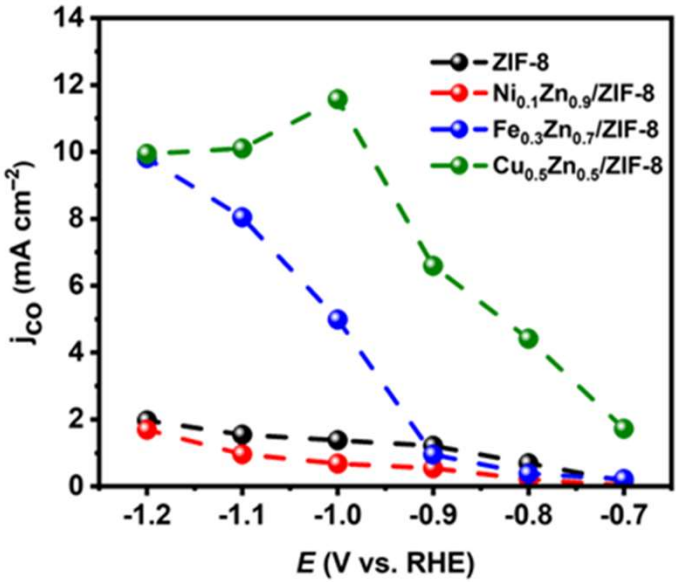

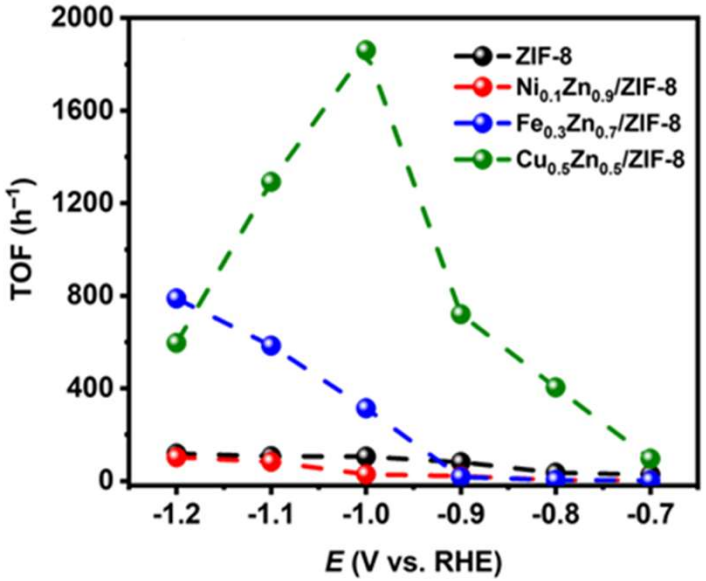

- Electrolyte : 0.5 M $KHCO_3$
- H-cell CO_2
- Flow rate : 20 mL/min

- $Cu_{0.5}Zn_{0.5}$/ZIF-8 and $Fe_{0.3}Zn_{0.7}$/ZIF-8 achieve a j_{total} of 17.6 and 29.2 mA cm^{-2} at -1.3 V vs. RHE.

- $Cu_{0.5}Zn_{0.5}$/ZIF-8 exhibits an FE_{CO} for 88.5% with high j_{CO} of 11.57 mA cm^{-2}.

- $Cu_{0.5}Zn_{0.5}$/ZIF-8 attains the best TOF of 1850 h^{-1}.

Electrochemical performance

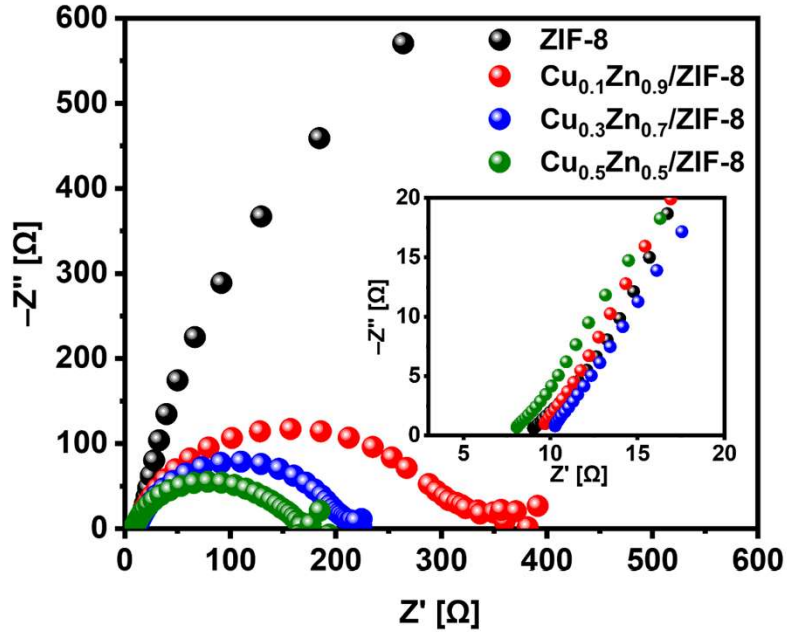

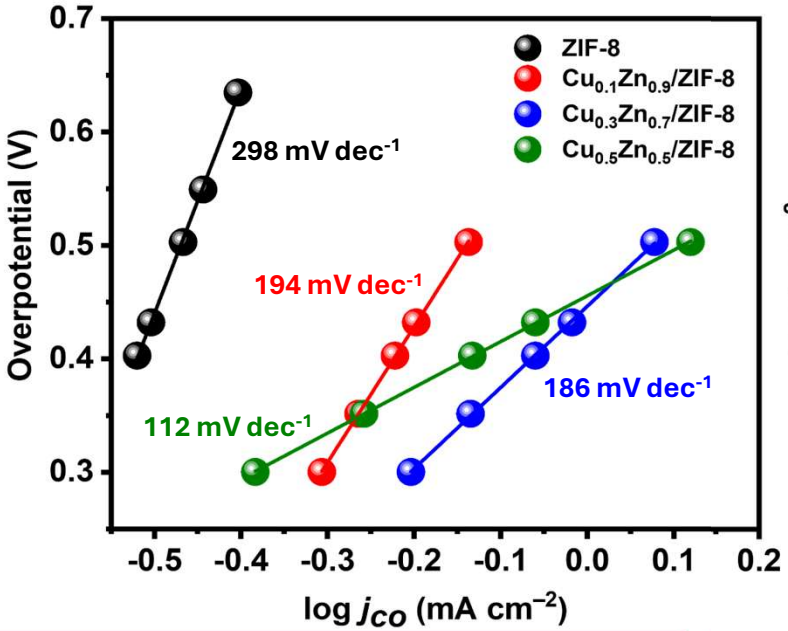

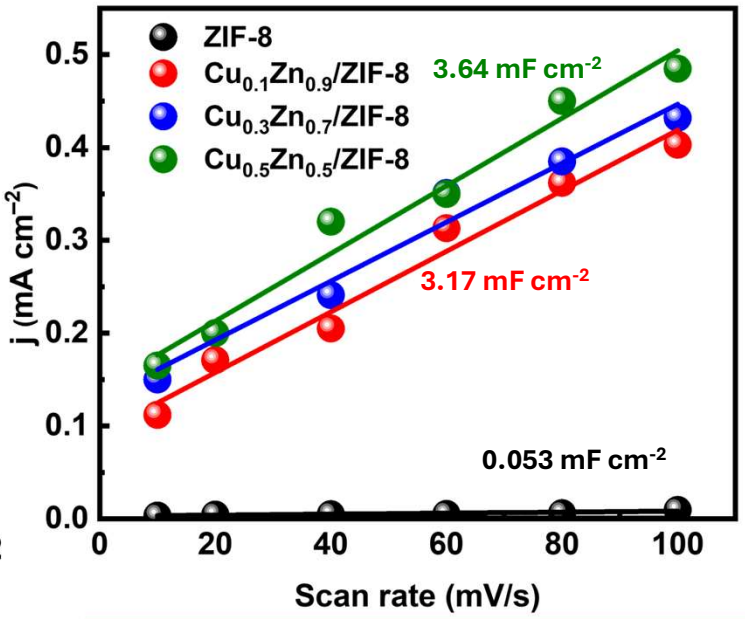

- From Nyquist plots, $Cu_{0.5}Zn_{0.5}$/ZIF-8 yields the **lowest charge-transfer resistance.**

- From Tafel slope, $Cu_{0.5}Zn_{0.5}$/ZIF-8 (112 mV dec^{-1}) are **favorable for COOH formation.**

- From ECSA, $Cu_{0.5}Zn_{0.5}$/ZIF-8 has **more electroactive sites** than ZIF-8.
(ECSA: Electrochemical Surface Area)

Theoretical Calculations

❖ **Simplified atomic structure of M_xZn_y/ZIF-8**

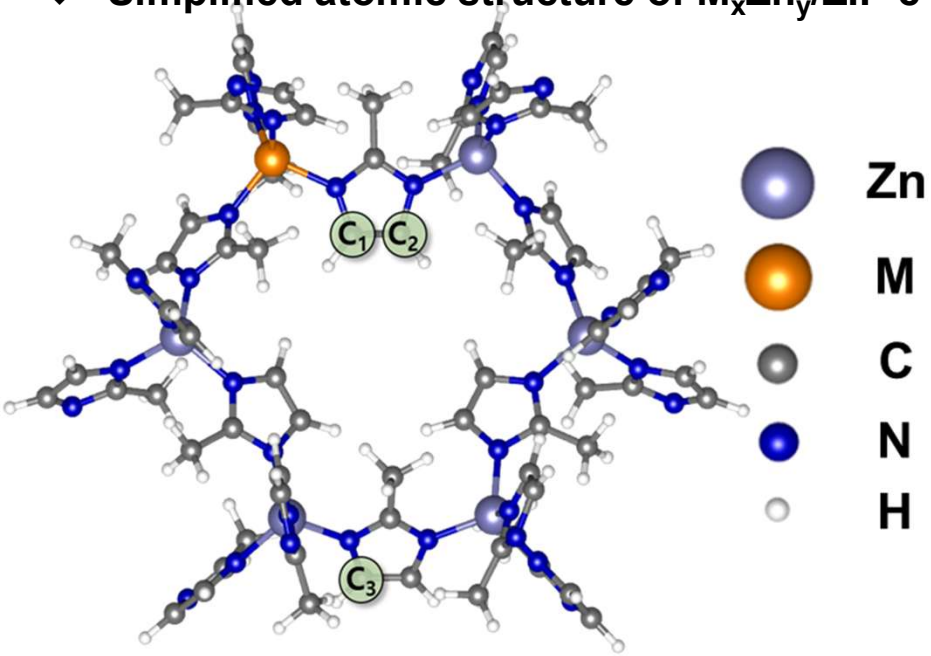

❖ **Gibbs free energy diagram of M_xZn_y/ZIF-8**

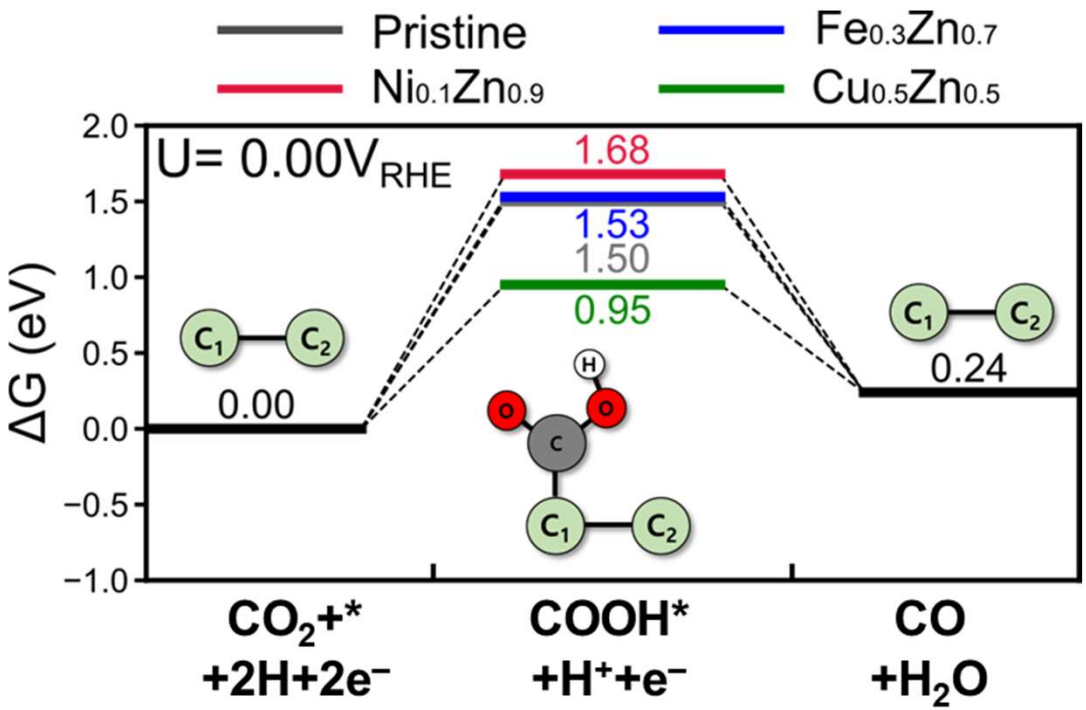

- sp^2 carbon sites of the imidazolate organic ligand bind adsorbates most strongly.
- Only, $Cu_{0.5}Zn_{0.5}$/ZIF-8 strengthens the COOH* binding (ΔG_{COOH^*}= 0.95 eV)

improves the catalytic activity and selectivity

Theoretical Calculations

OSPL
Organic Semiconductor Process Lab.

❖ **Gibbs free energy diagram under H-covered state**

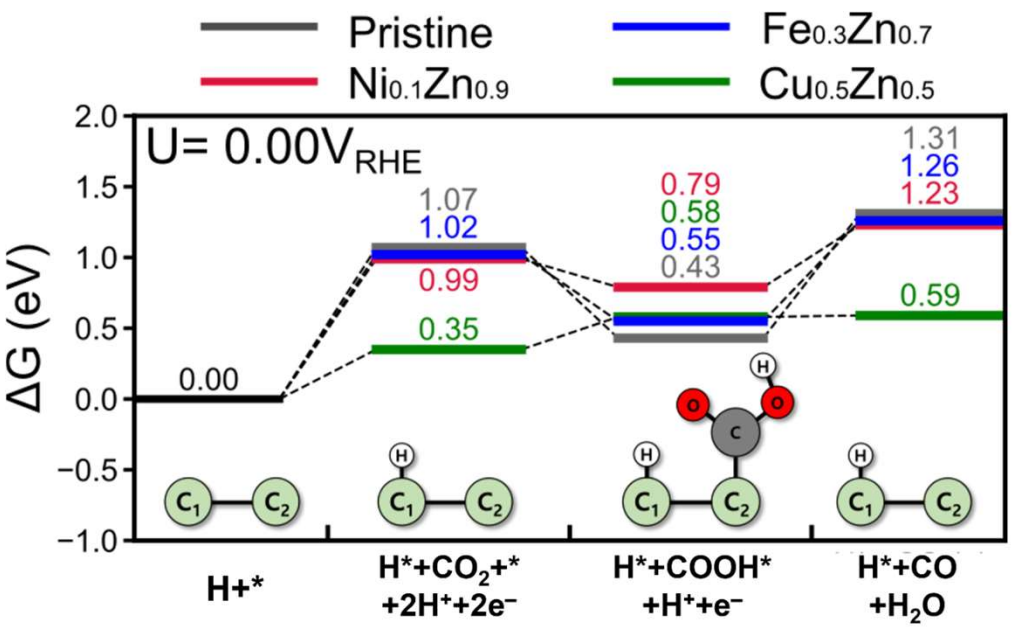

❖ **Limiting potential for M_xZn_y/ZIF**

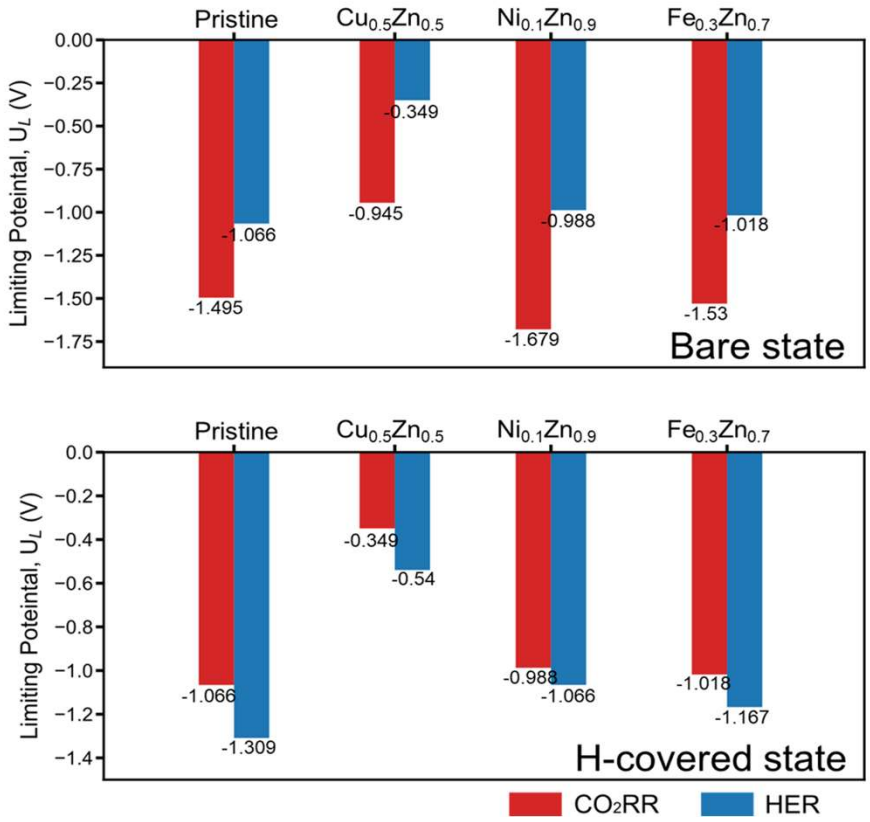

- Stronger H* binding on $Cu_{0.5}Zn_{0.5}$/ZIF-8 renders the H-covered state more favorable than the bare state under CO_2RR conditions (U < –0.35 V).
- H-covered state demonstrates that CO_2RR is **downhill** in the case of $Cu_{0.5}Zn_{0.5}$/ZIF-8, resulting in a less negative **U_L,CO_2RR (–0.35 V)** than **U_L,HER (–0.54 V).**

Theoretical Calculations

OSPL
Organic Semiconductor Process Lab.

❖ **PDOS of Pristine ZIF-8**

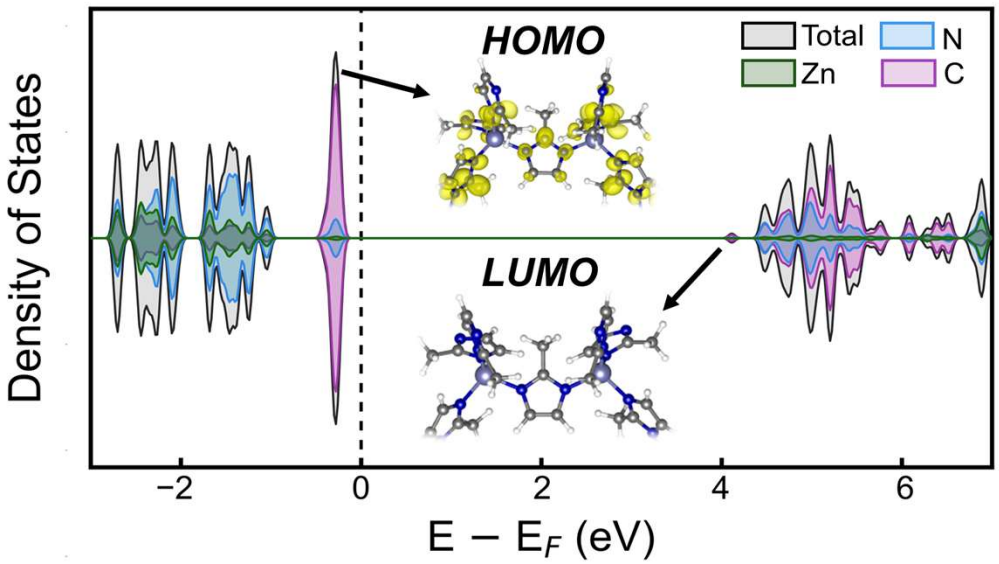

❖ **PDOS of Pristine Cu doping on ZIF-8**

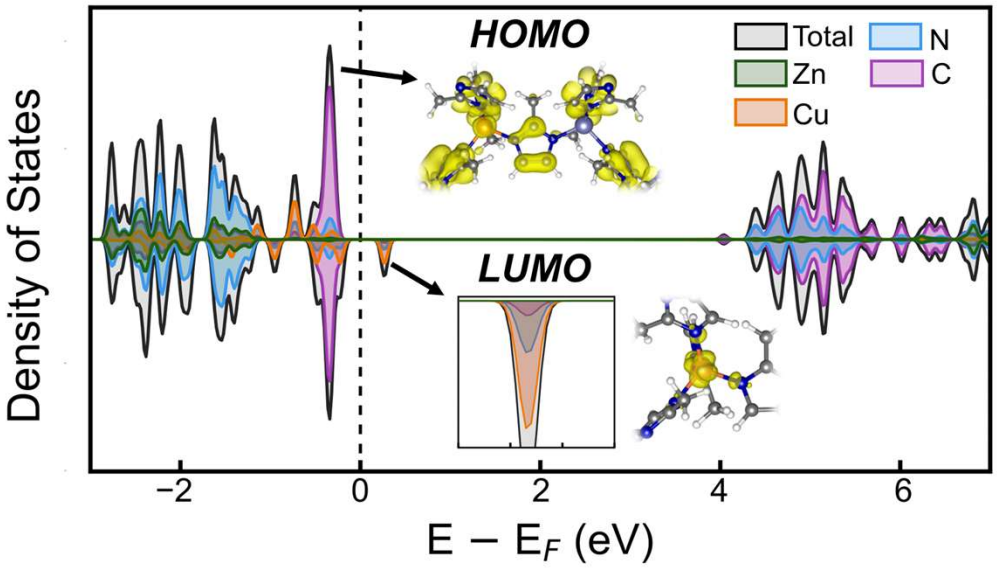

- The partial density of states (PDOS) shows that additional electronic states are introduced upon **Cu doping, reducing the gap** between the HOMO LUMO, facilitating electron transfer
- Electron density distributions of the HOMO demonstrate that active carbon sites become highly **electron-rich** when Cu is doped, rendering them highly active toward **COOH* binding.**

Summary

One-step facile synthesis process

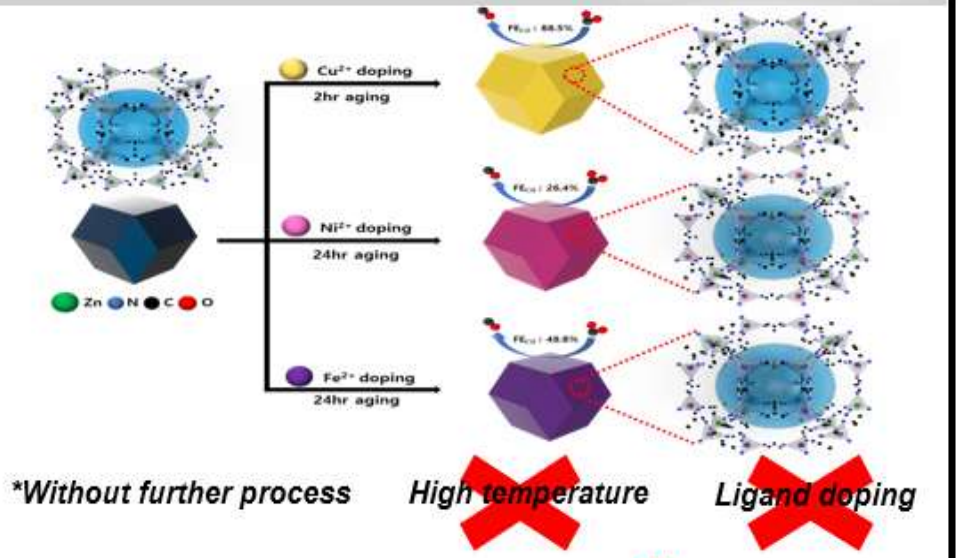

*Without further process High temperature Ligand doping

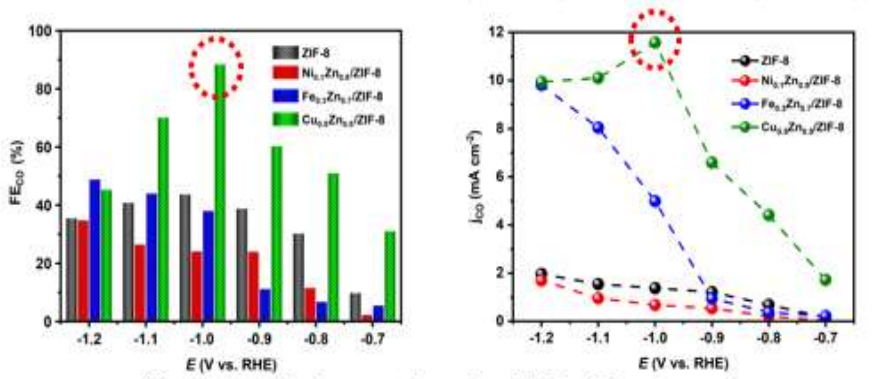

*Enhanced electrochemical CO_2RR properties

Unveiling active site of CO_2RR electrocatalyst

Preabsorbed Hydrogen covered state

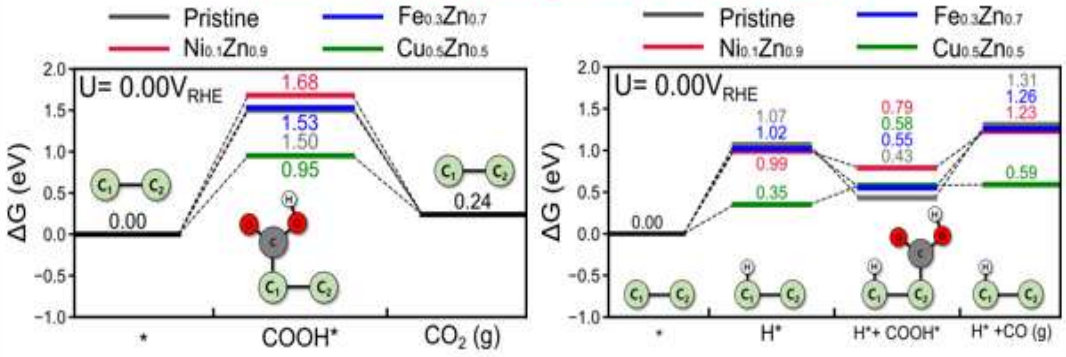

Affected on the electronic structure

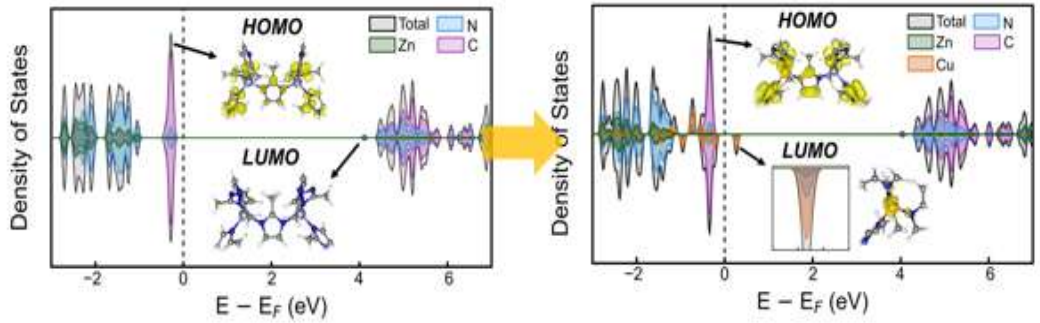

*By reducing the gap between HOMO and LUMO

Advanced Materials, 35, p.2208224 (1-9) (2023)

Single-atom Catalysts

Low price !
High efficiency !

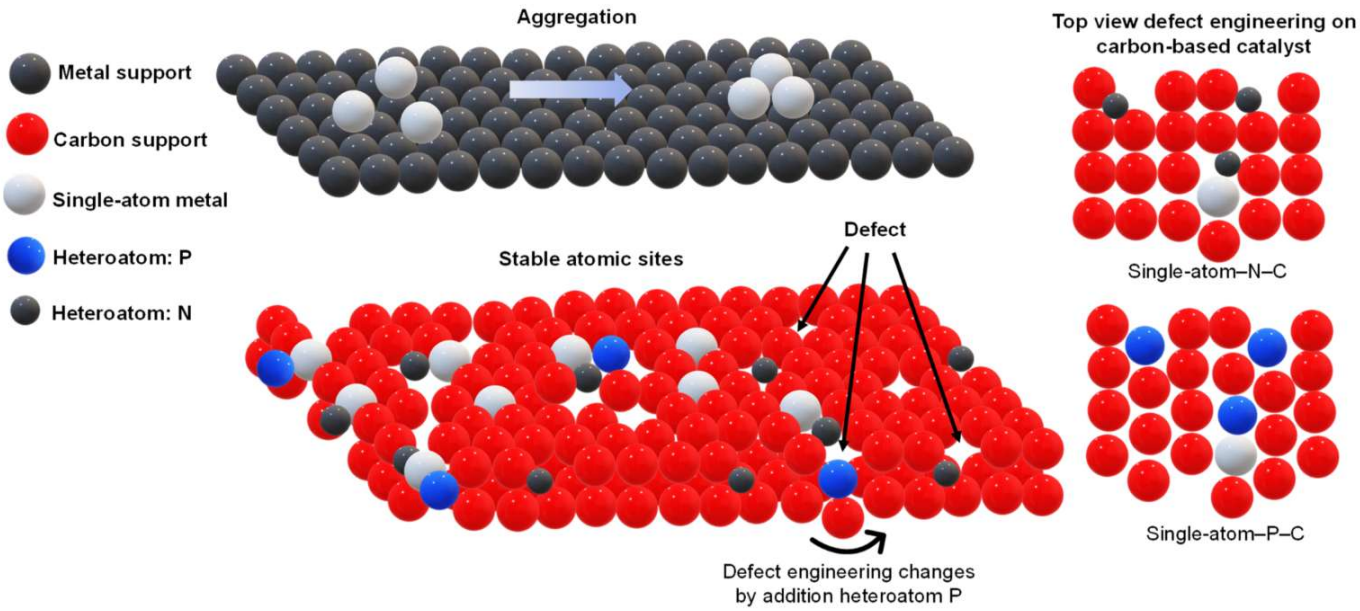

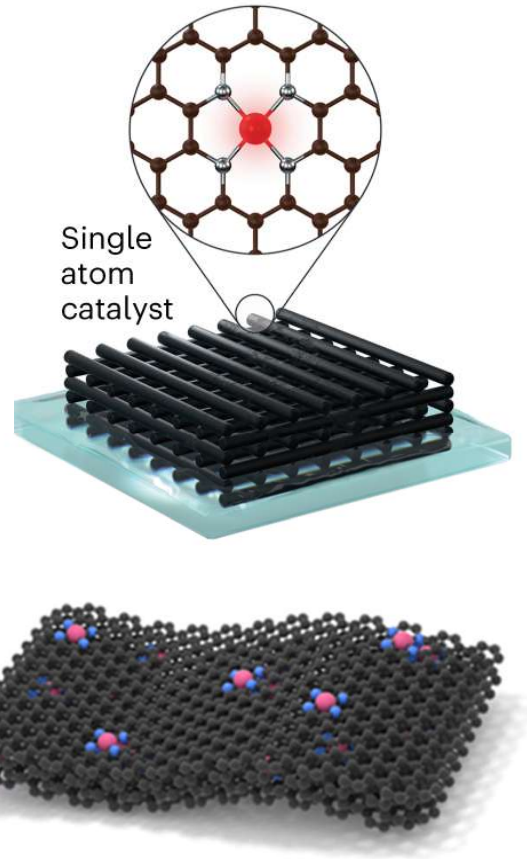

- SACs, a cutting-edge field in catalyst science, involves isolating metal atoms on suitable carriers or supports.
- SACs offer high efficiency and atom utilization.
- Application: energy conversion, organic catalysis, biocatalysis, photocatalysis, electrocatalysis

Single-atom Catalysts

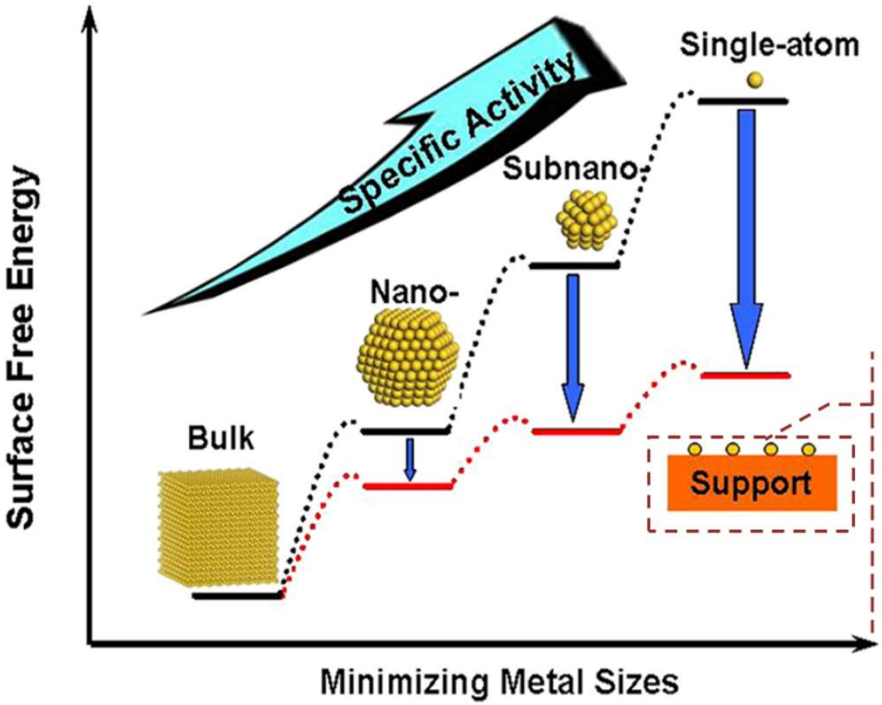

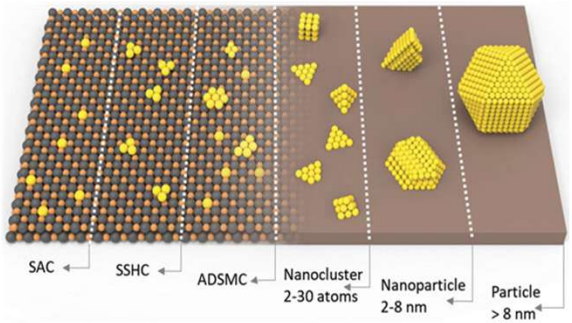

Support Candidates

1) Graphene
2) Graphene Oxide (GO)
2) g-C_3N_4
3) Metal Organic Frameworks (MOF)

Advantages

- Maximum atom utilization
- Fully exposed, highly selective, and well-defined active sites
- Outstanding catalytic activity and stability

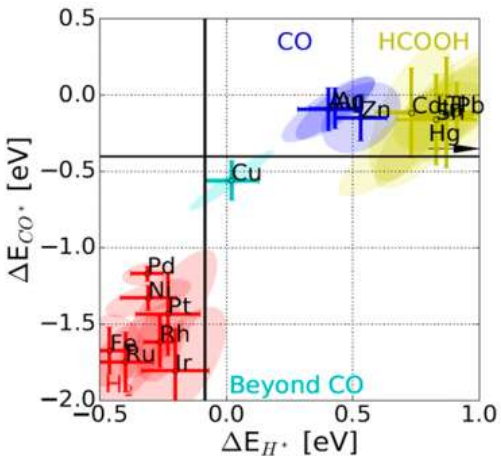

ChemPhysChem 18 (2017) 3266.

Bulk/nano catalysts	Main products
Pt, Pd, Ru, Ni, Co…	H_2
Au, Ag, Zn	CO
Sn, In, Pb…	HCOOH
Cu	H_2, CO, HCOOH, C_2H_4, C_2H_6, CH_3COOH…

Conventional selectivity

Single atom catalysts	Main products
Pt, Ni, Co…	H_2
Ni, Co, Fe, Mn, Zn, Sn	CO
Mo	HCOOH
Cu	CO, CH_4, CH_3OH, C_2H_4, C_2H_6, C_2H_5OH…

Unexpected selectivity

Curr. Opin. Green Sustain. Chem. 16 (2019) 1
Environ. Chem. Lett. 18 (2020) 1595.

Experimental Methods

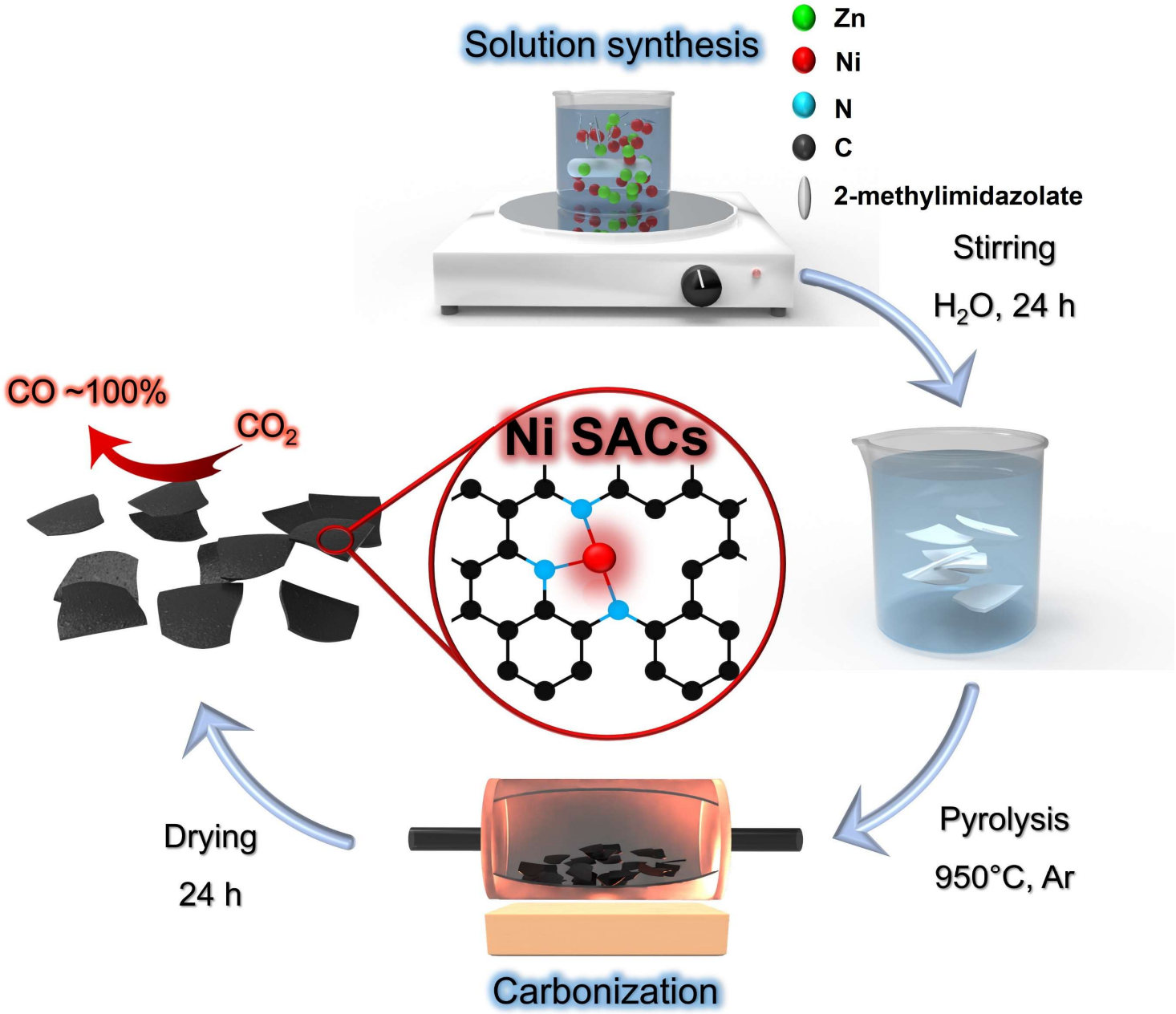

Characterizations

ZIF-8-NS

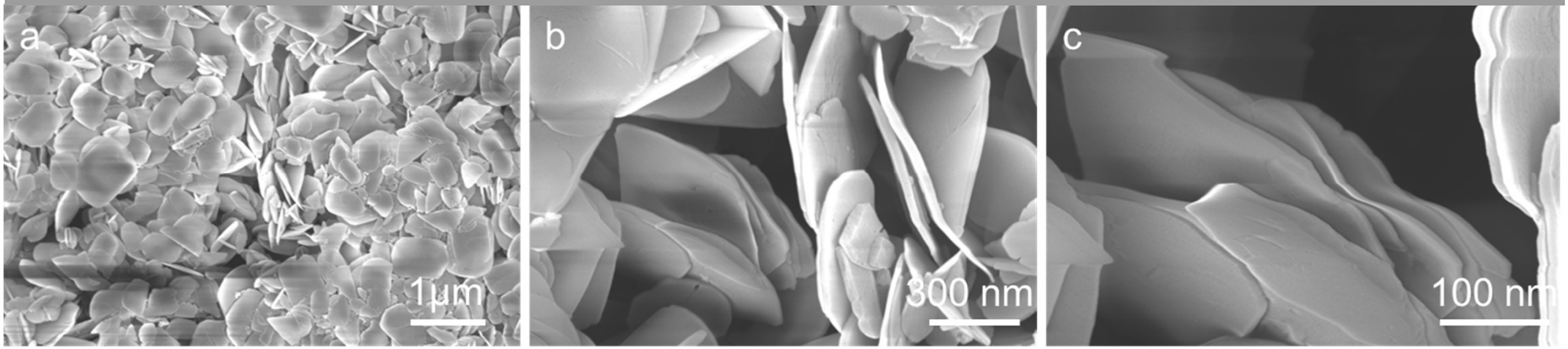

Ni-ZIF-8-NS

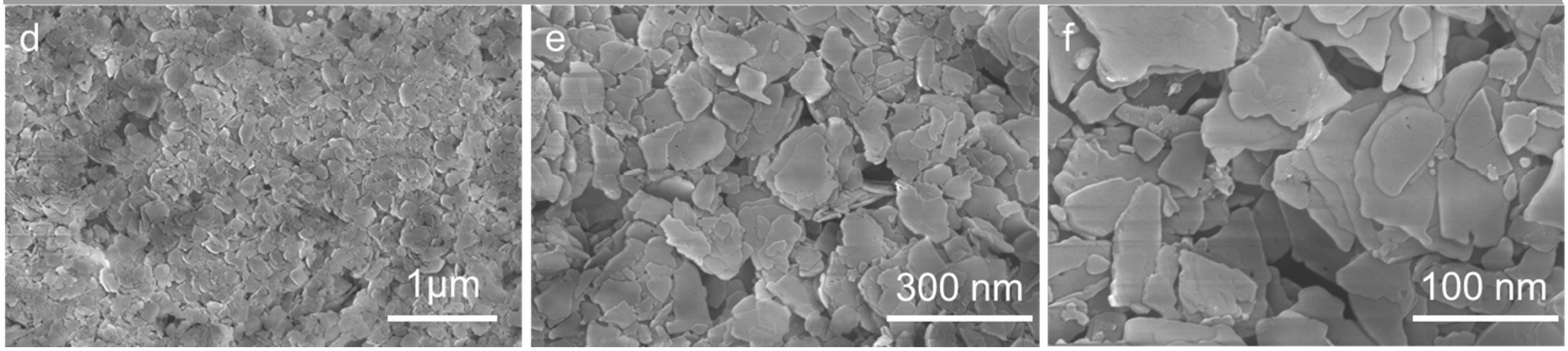

Characterizations

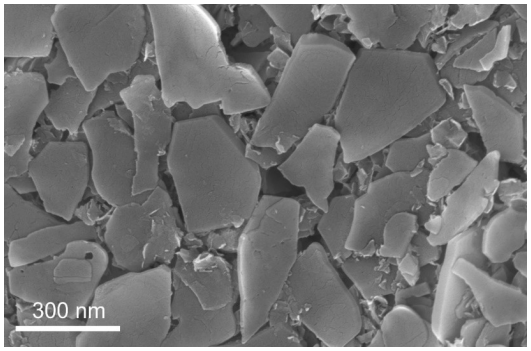

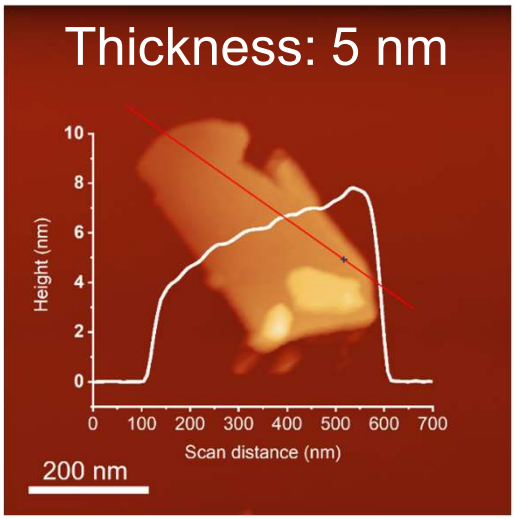

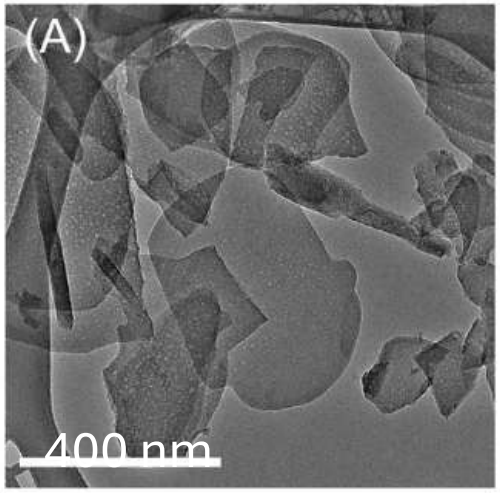

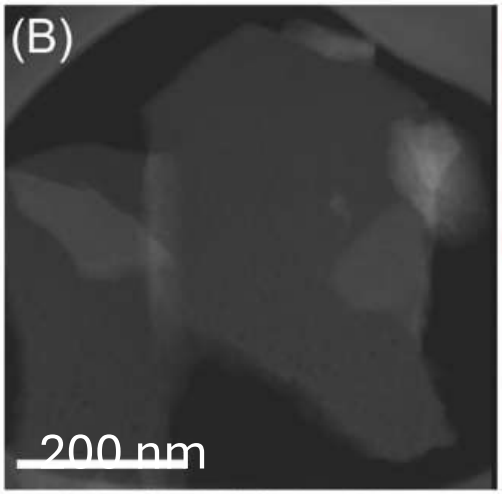

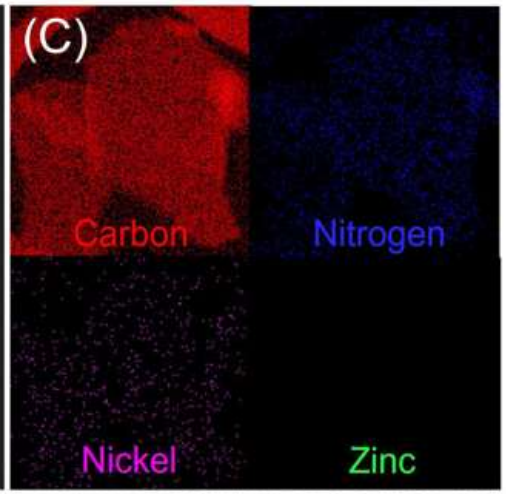

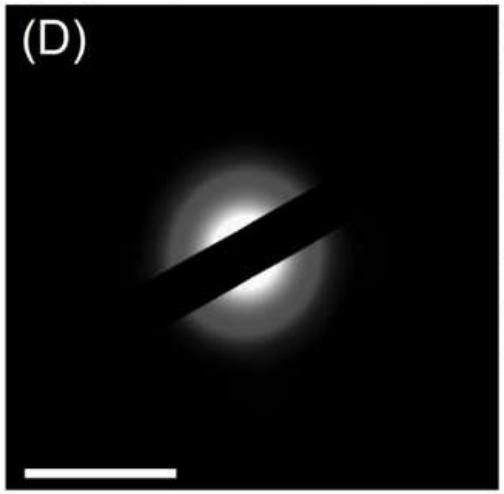

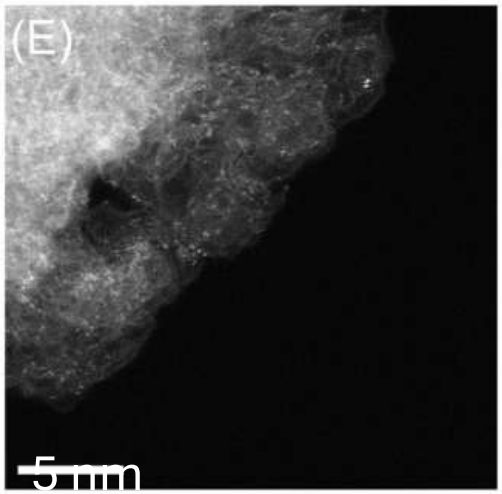

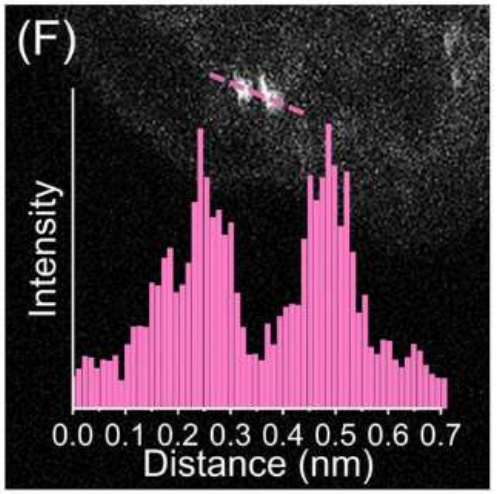

- Ni-NC-NS exhibits a nanosheet morphology with an area of ~300 nm.
- EDS mapping profiles show the well-dispersed Ni, N, and C elements in porous graphitic carbon nanosheet structure. (Zn signals are not detected.)

Characterizations

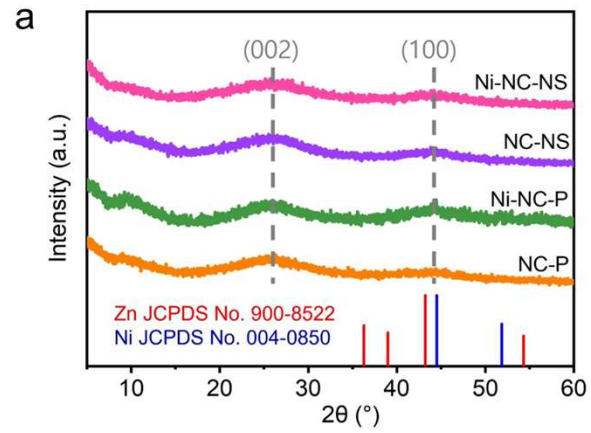

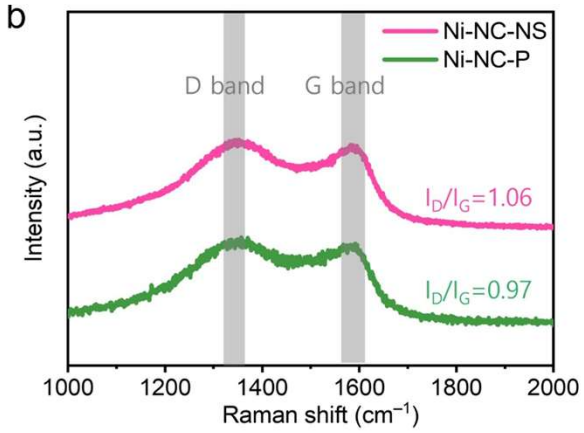

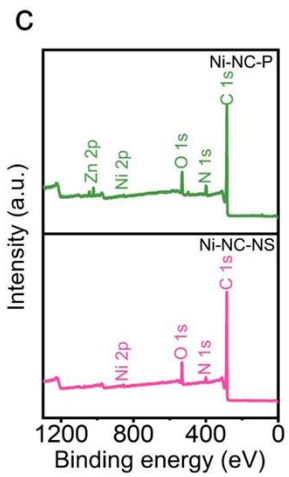

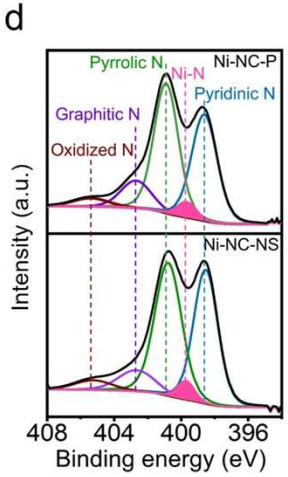

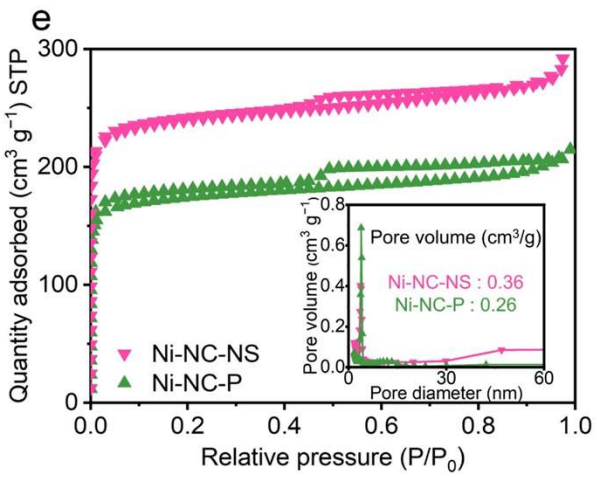

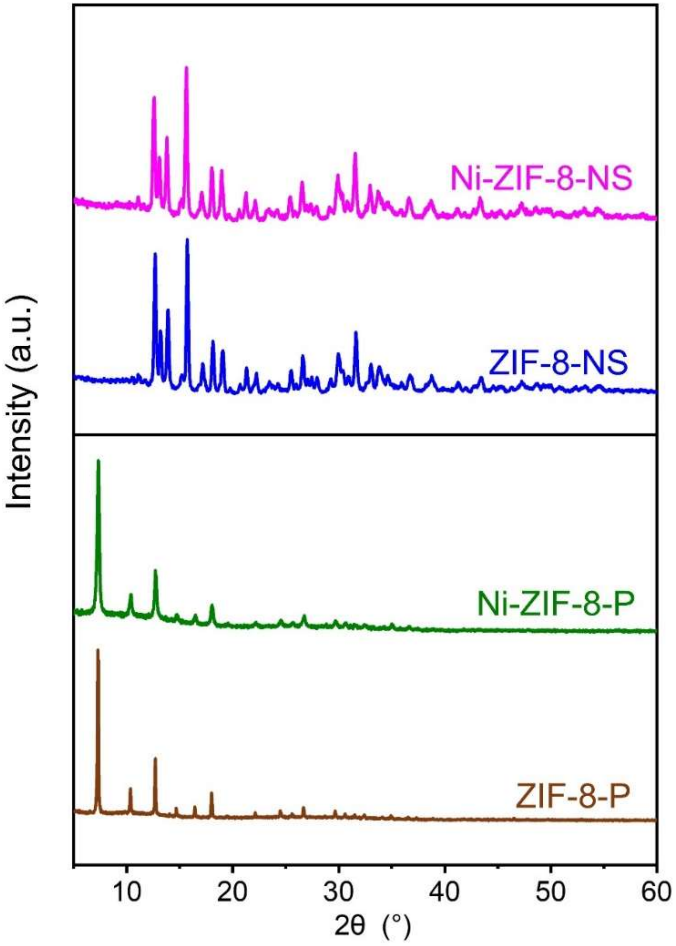

- Raman spectra depict a higher I_D/I_G ratio of Ni-NC-NS (1.06) than Ni-NC-P (0.97).
- Zn is only detected in the Ni-NC-P (XPS); consistent with aforementioned EDS result.
- A specific surface area of 930 $m^2\ g^{-1}$ with a pore volume of 0.36 $cm^3\ g^{-1}$ for Ni-NC-NS.

Characterizations

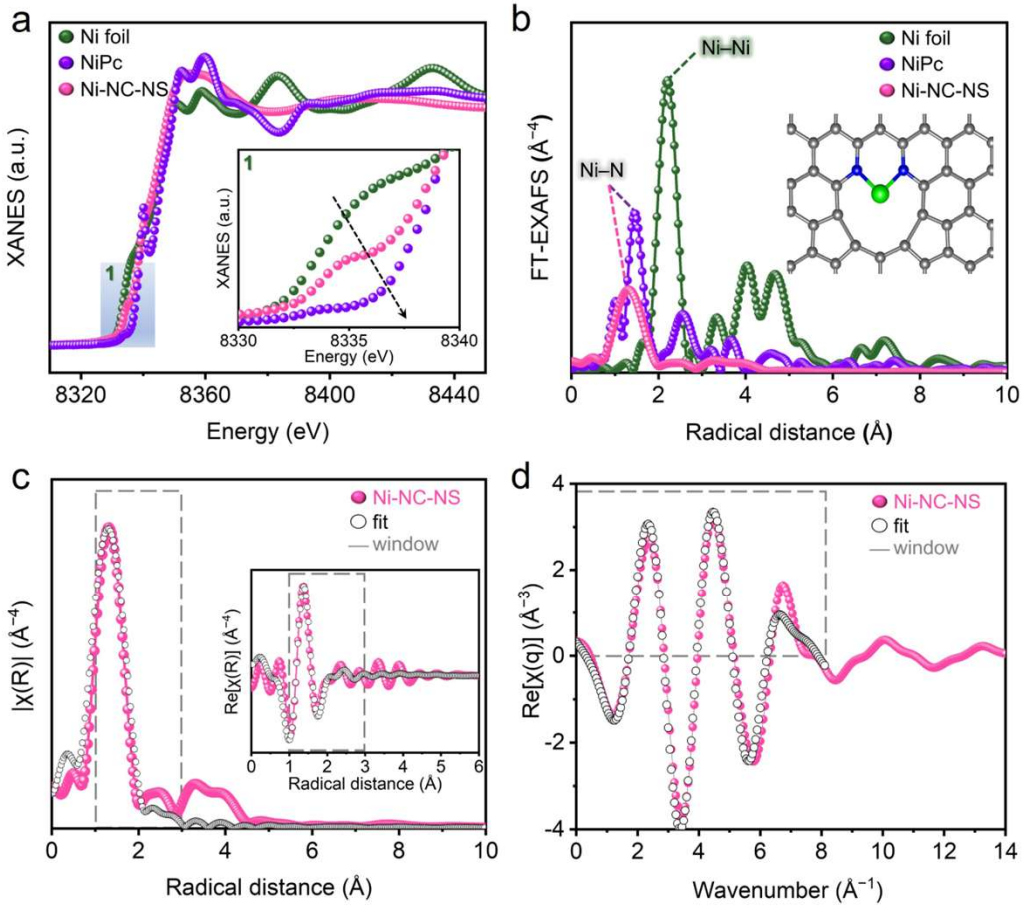

Table S3. Ni K-edge extended X-ray absorption fine structure curve fitting parameters for reference and electrocatalysts.

Sample	*Path*	*CN*[a]	*R (Å)*[b]	*σ² (10⁻³ Å²)*[c]	*R_f*[d]
Ni foil	Ni–Ni	12	2.480	6.0	0.003
NiPc	Ni-N	4	1.910	3.7	0.004
Ni-NC-NS	Ni-N	2.3 ± 0.1	1.812	4.2	0.005
Ni-ZIF-8-NS	Ni-N	4	1.880	3.1	0.003
Ni-NC-P	Ni-N	3.2 ± 0.2	1.845	3.2	0.005

[a]CN, coordination number; [b]R, an interatomic distance of the bond length between absorber and backscatter atoms); [c]σ2, Debye–Waller factor accounts for both thermal and structural disorders in the absorber–scatter distance; [d]R_f factor (%) indicates the quality of EXAFS fitting.

Table S4. Zn K-edge extended X-ray absorption fine structure curve fitting parameters of Ni-NC-P.

Sample	*Path*	*CN*[a]	*R (Å)*[b]	*σ² (10⁻³ Å²)*[c]	*R_f*[d]
Ni-NC-P	Zn-N	3.6 ± 0.4	1.985	4.1	0.004

- Ni valence state of Ni-NC-NS from XANES spectra: $Ni^{\delta+}$ nature ($0 < \delta < 2$)
- Ni-N coordination number: Ni-NC-NS (2.3) Ni-NC-P (3.2)
- Zn-N coordination number: Ni-NC-NS (X) Ni-NC-P (3.6)

Electrochemical performance

OSPL
Organic Semiconductor Process Lab.

H-cell reactor

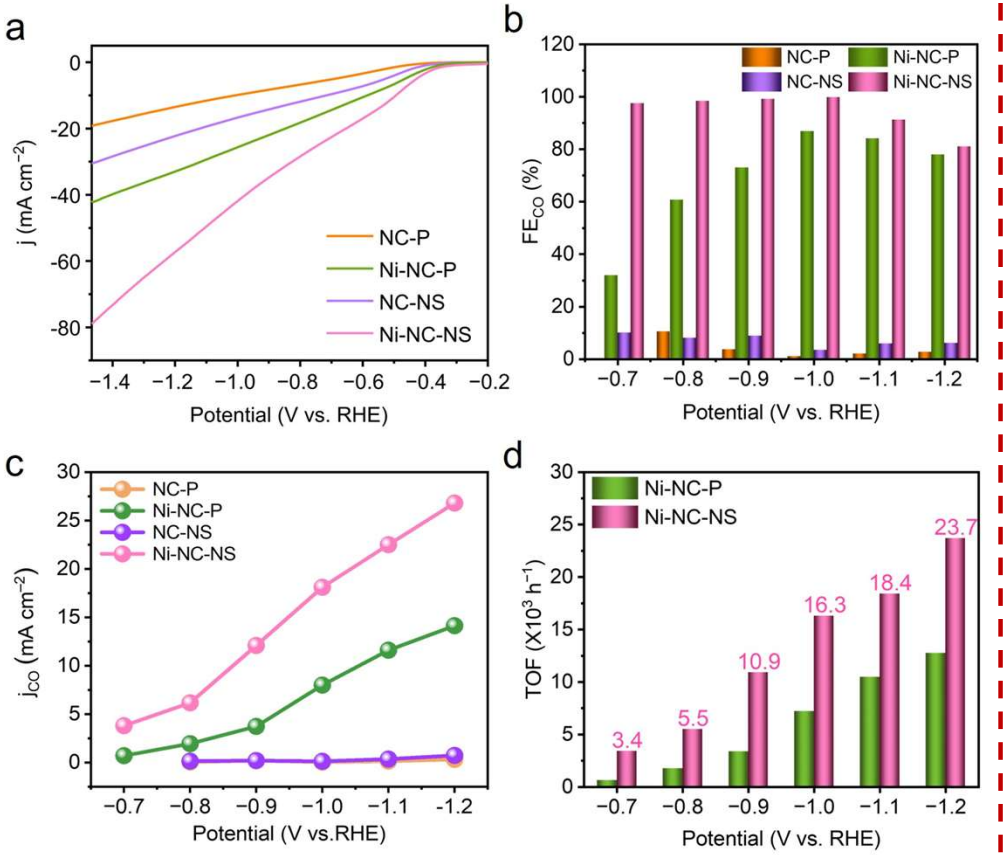

Flow-cell reactor

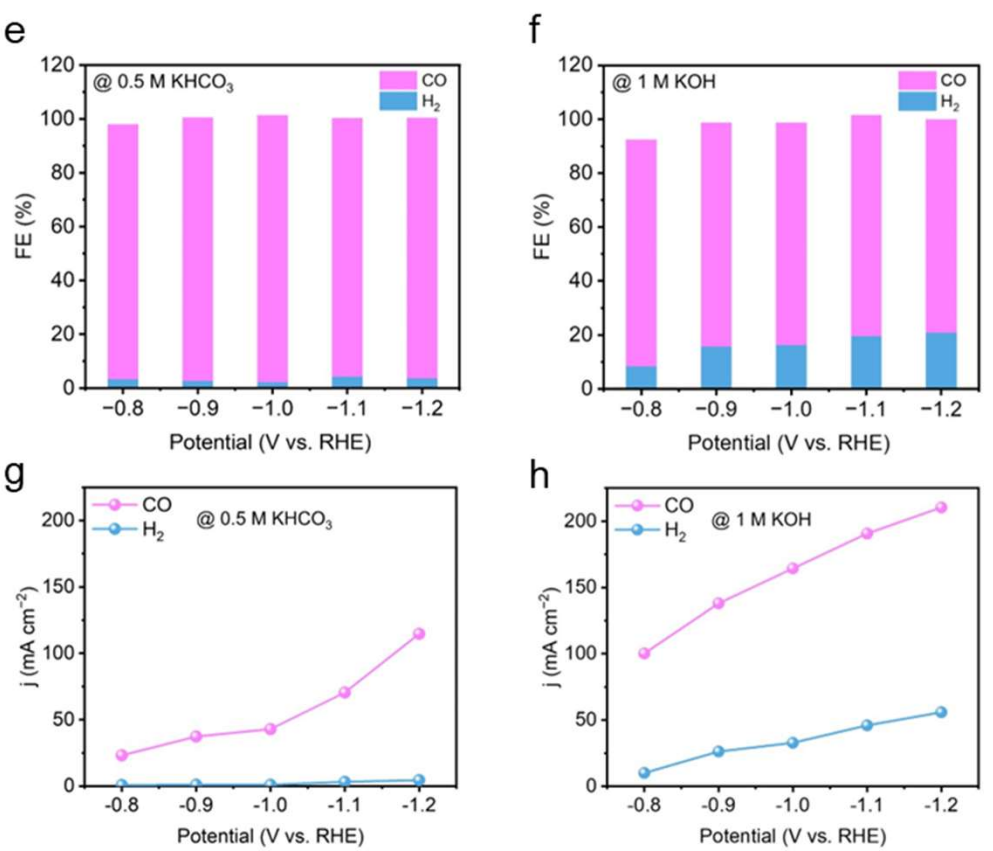

- Ni-NC-NS achieves the FE_{CO} of ~100%, and high CO partial current density (26.8 mA cm^{-2}).
- TOF: Ni-NC-NS (23,699 h^{-1}), Ni-NC-P (12,000 h^{-1}) at -1.2 V vs RHE.
- FE_{CO} of over 94% / in 1 M KOH; j_{CO} of 210 mA cm^{-2}

Theoretical Study

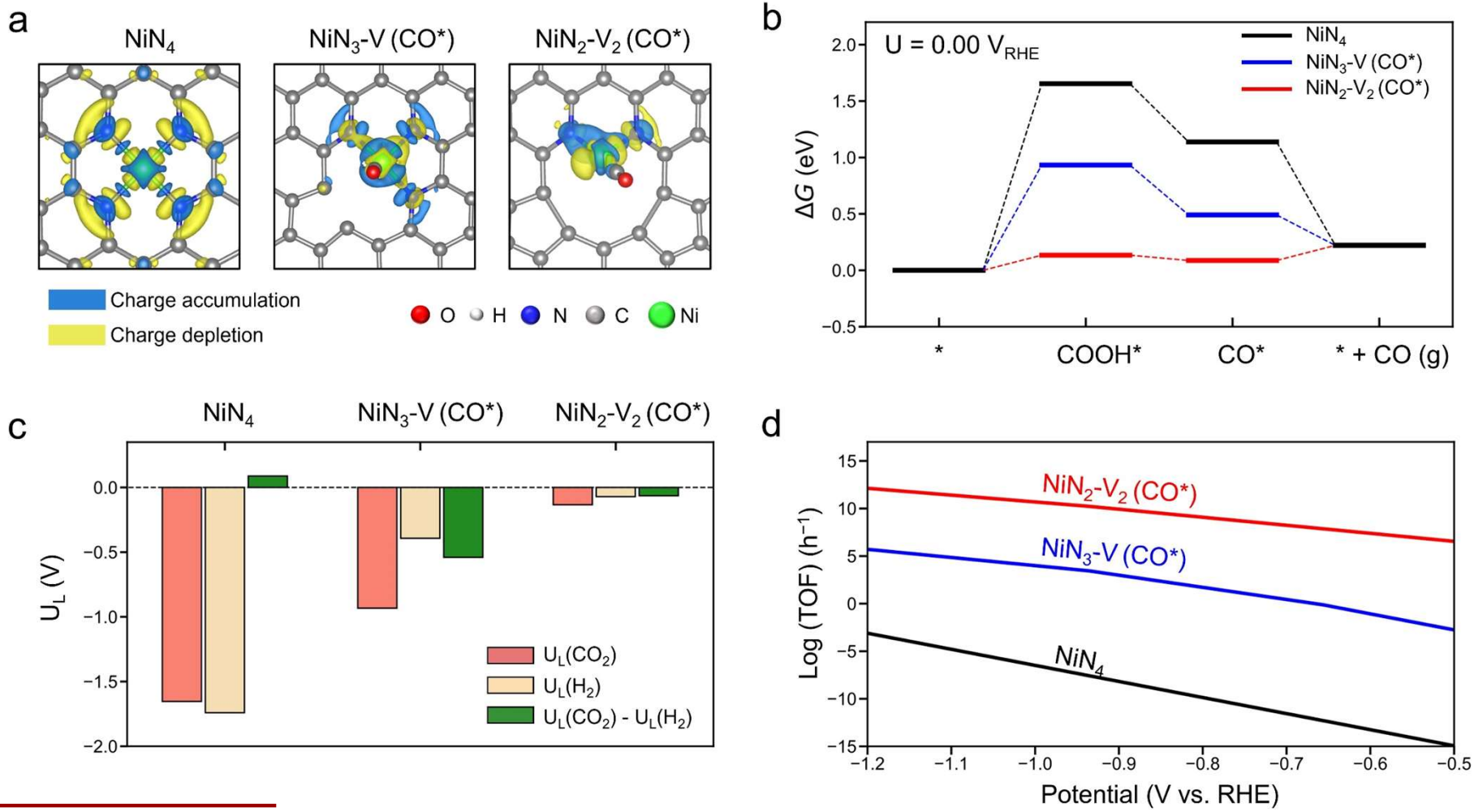

- Ni-NC-NS: NiN_2-V_2 (major) + NiN_3-V (minor) / Ni-NC-P: NiN_3-V (major) + NiN_2-V_2 (minor)
- CO* pre-adsorbed sites as the initial states
- Limiting potential: U_L (CO_2)) – U_L (H_2) / NiN_2-V_2 exhibited the most favorable U_L

Theoretical Study

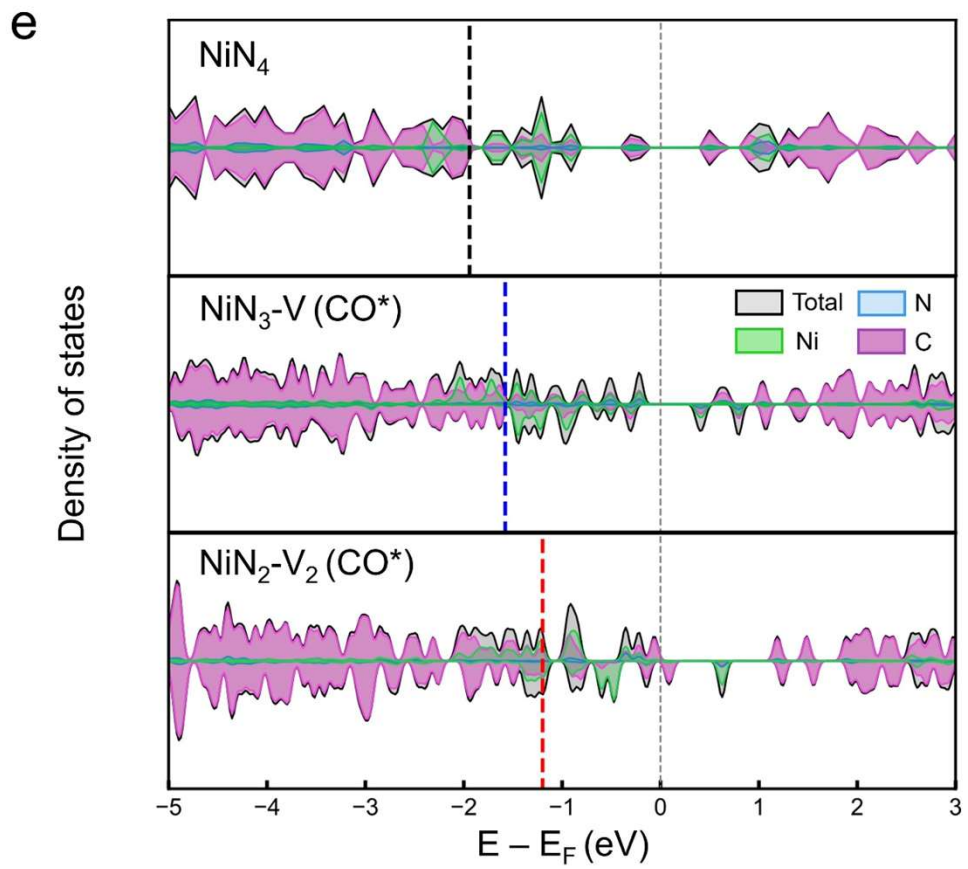

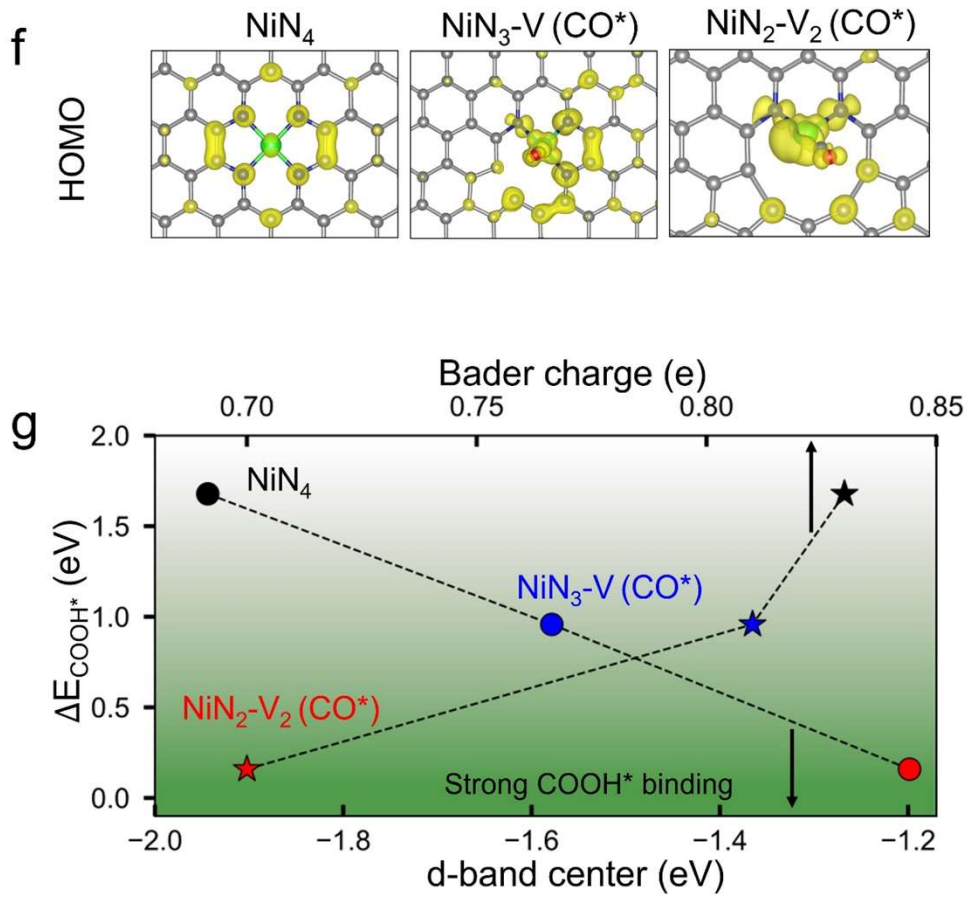

- d-band center: NiN_4 (-1.94 eV), NiN_3-V (-1.58 eV), NiN_2-V_2 (-1.20 eV)
- NiN_2-V_2 (-1.20 eV): less electron occupation of antibonding states, stronger COOH binding and facilitates the activation of CO_2.
- HOMO show more localized electron density, as the number of vacancy sites increases.

Summary

2D MOF nanosheet as SACs support

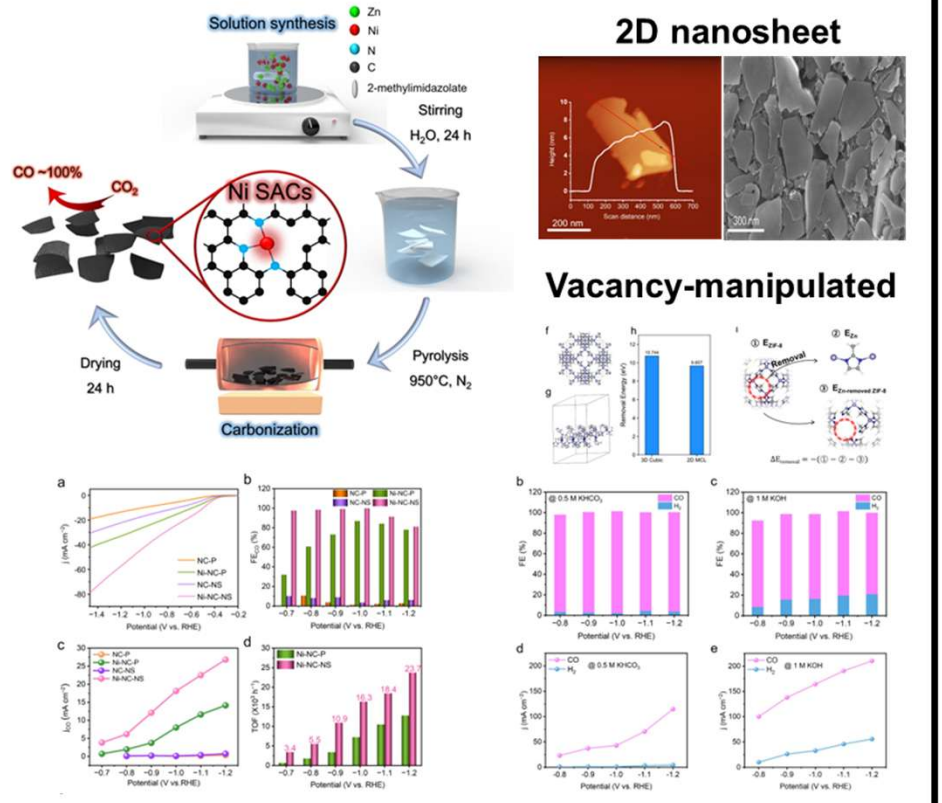

Unveiling active site of CO_2RR electrocatalyst

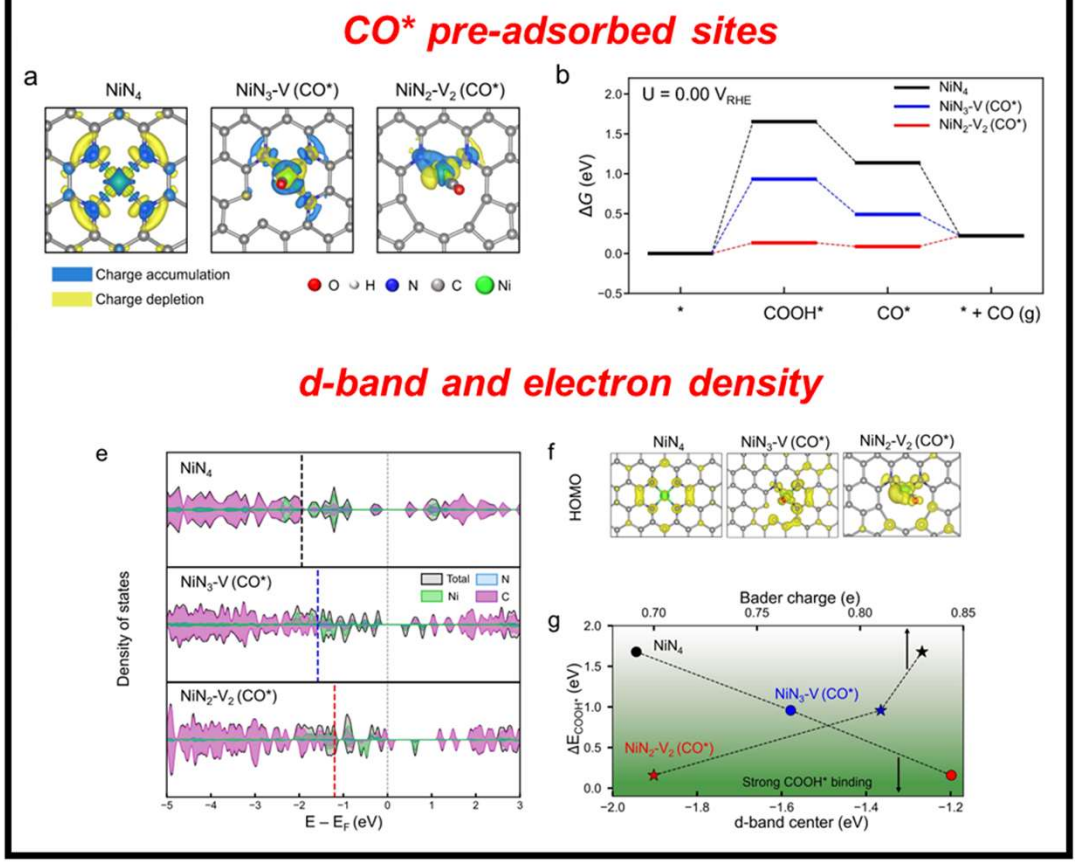

Carbon Energy vol.6, p.e510 (2024)

Challenge of metal aggregation

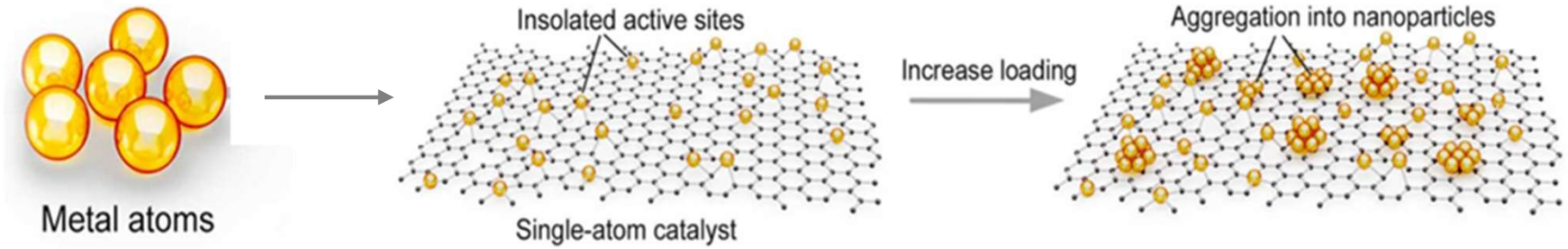

Materials Today Catalysis 1 (2023): 100004.

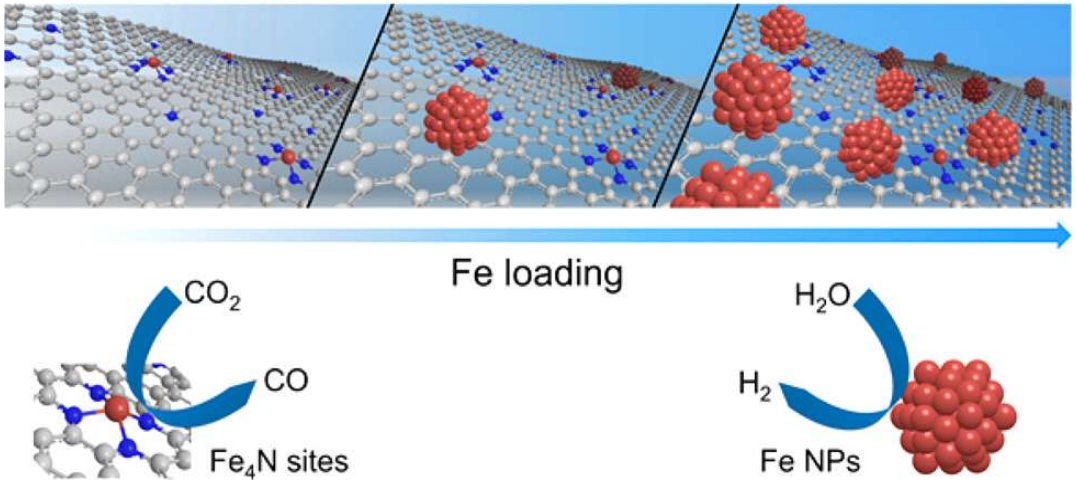

ACS catalysis 7.3 (2017): 1520-1525.

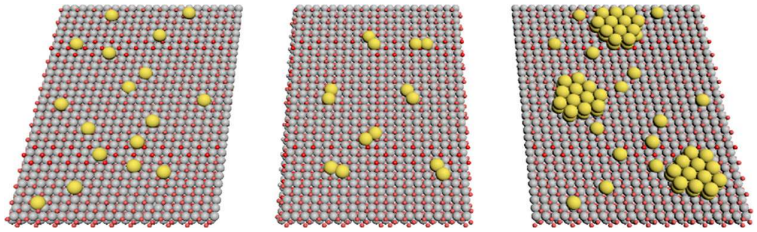

J. Am. Chem. Soc.144.40 (2022): 18155-18174.

- Due to the high surface energy of single atoms, stabilizing them against **atomic migration** and **aggregation** is quite challenging.
- Furthermore, SACs typically face the limitation of their **low metal loading**, limiting their accessible active sites.

Metal-chelating ligand strategy

OSPL
Organic Semiconductor Process Lab.

1,10 phenanthroline

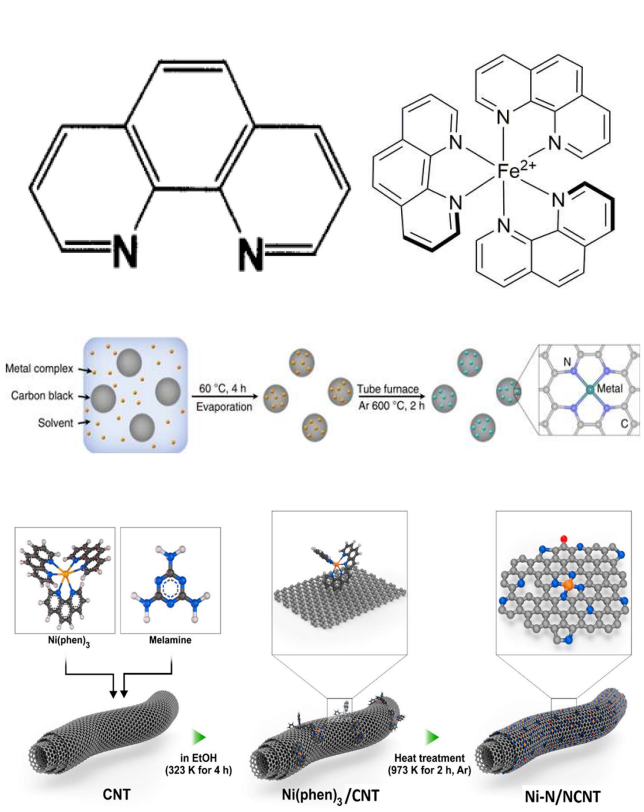

Citric acid

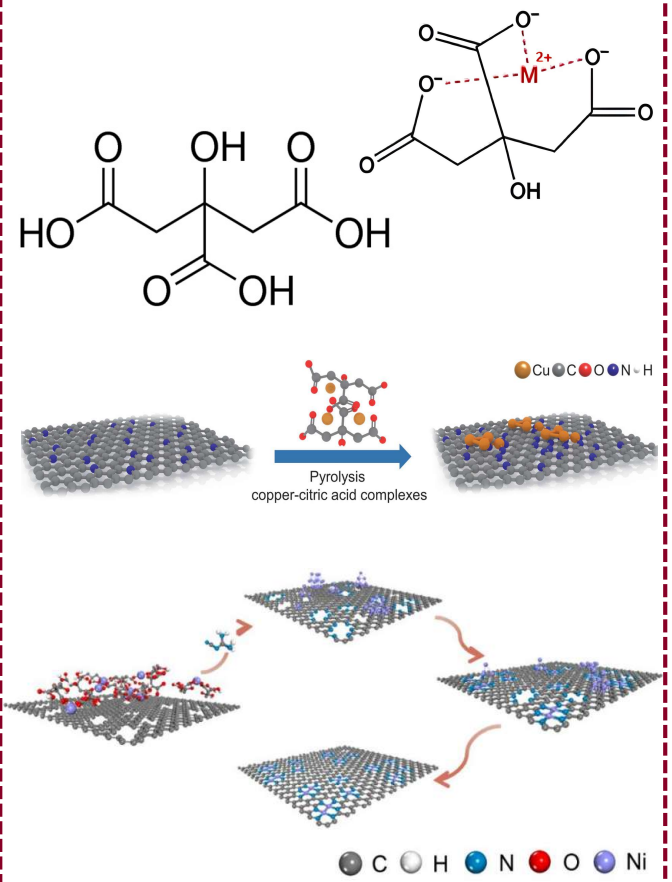

α-D-glucose

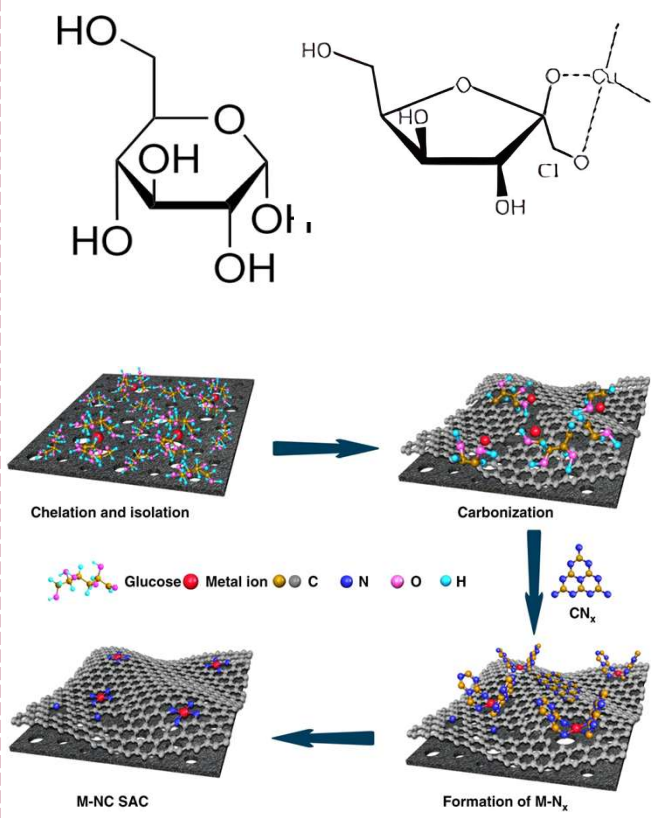

Abundant hydroxyl or amine groups can chelate metal ions
→ Metal-ligand complex

Metal-chelating ligand strategy

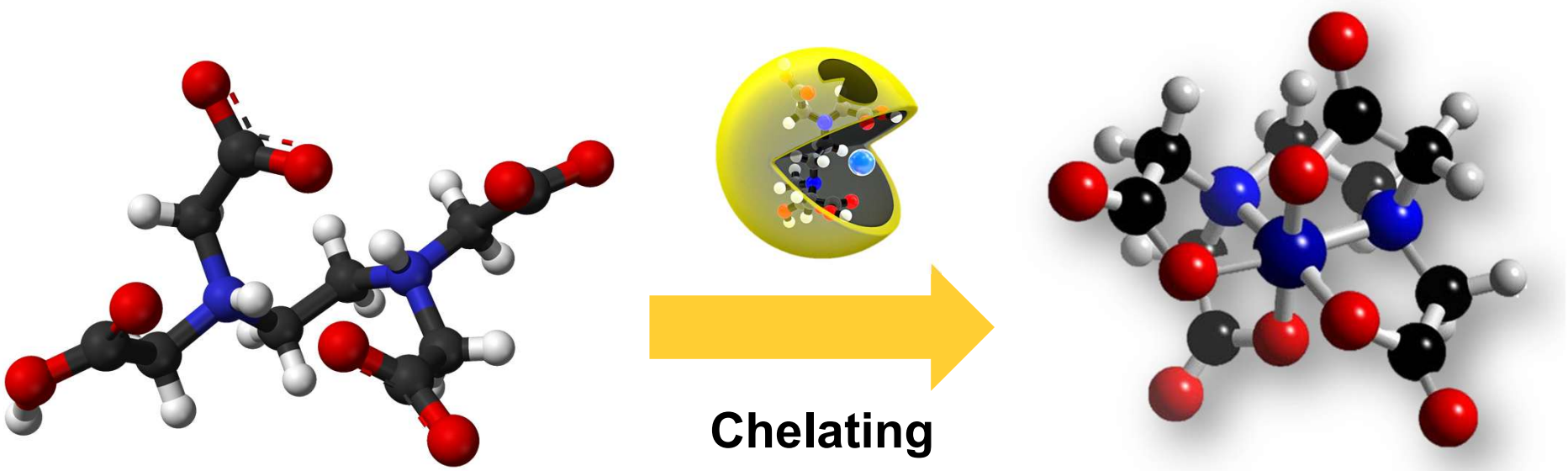

EDTA

Chelating metal ions

Metal-EDTA complex

- **EDTA** exhibits strong metal chelating properties due to its structural characteristics.
  (EDTA: ethylene-diamine-tetraacetic acid)
- It is a **hexadentate ligand** (4 carboxylate & 2 amine groups) capable of forming stable complexes with metal ions.
- This enables it to effectively **sequester metal ions**, separating them from solvents or other substances.

A suitable ligand candidate for the metal-chelating ligand strategy

Experimental Methods

Facile & Cost-effective synthesis strategy

Structure of Ni-EDTA complex

OSPL
Organic Semiconductor Process Lab.

Ni-EDTA complex

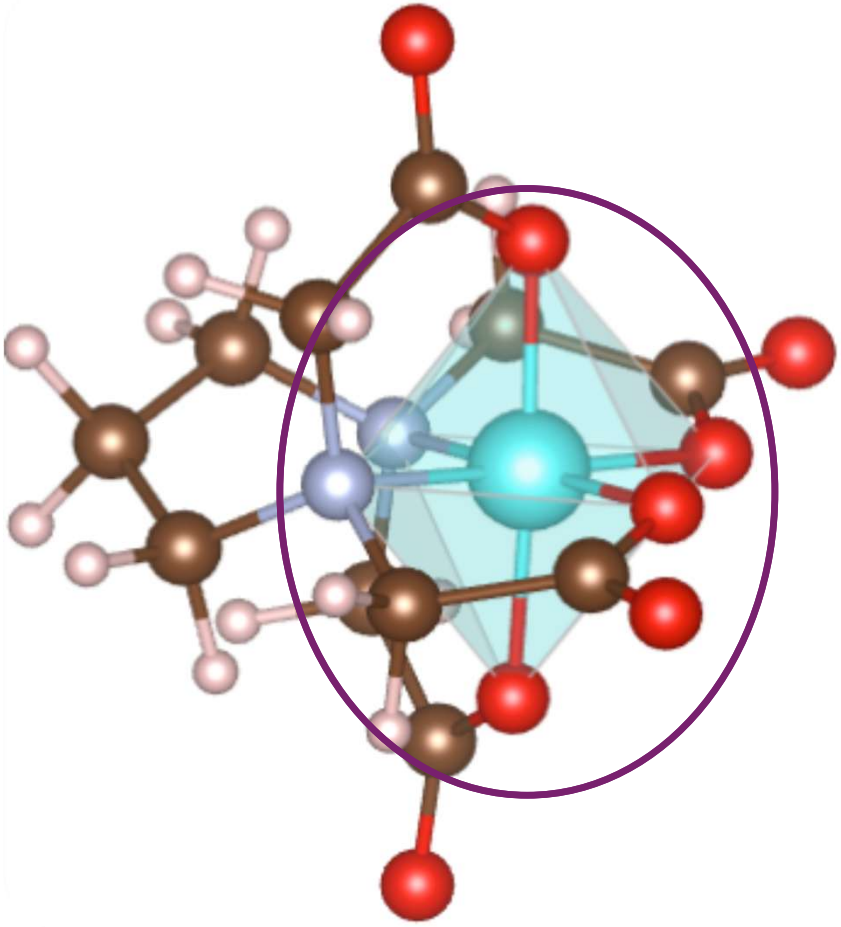

Distorted centrosymmetric structure

UV-vis & XAFS

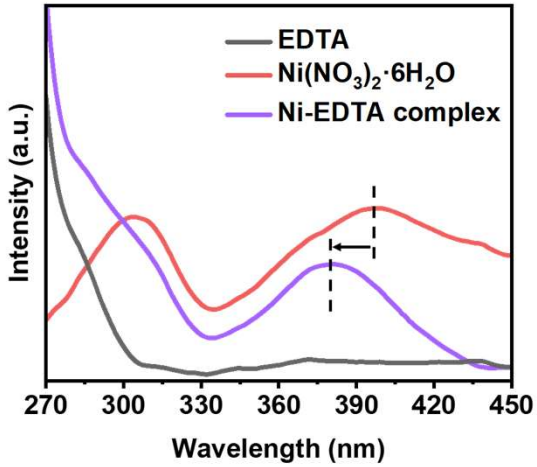

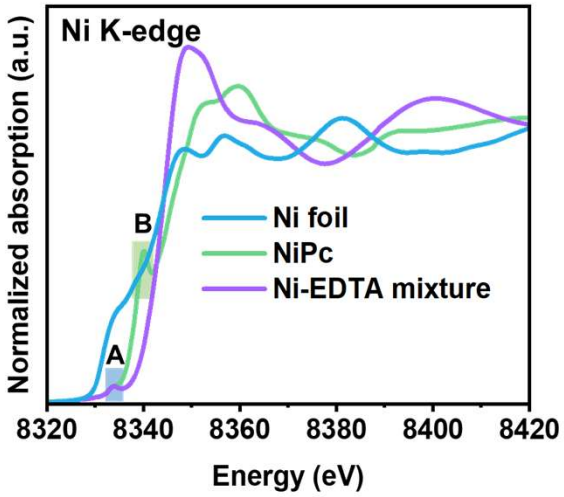

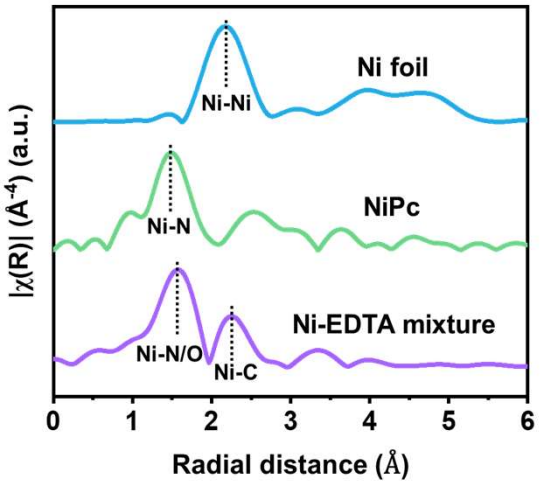

Successful formation of the Ni-EDTA complex

Characterizations

E-Ni-NC

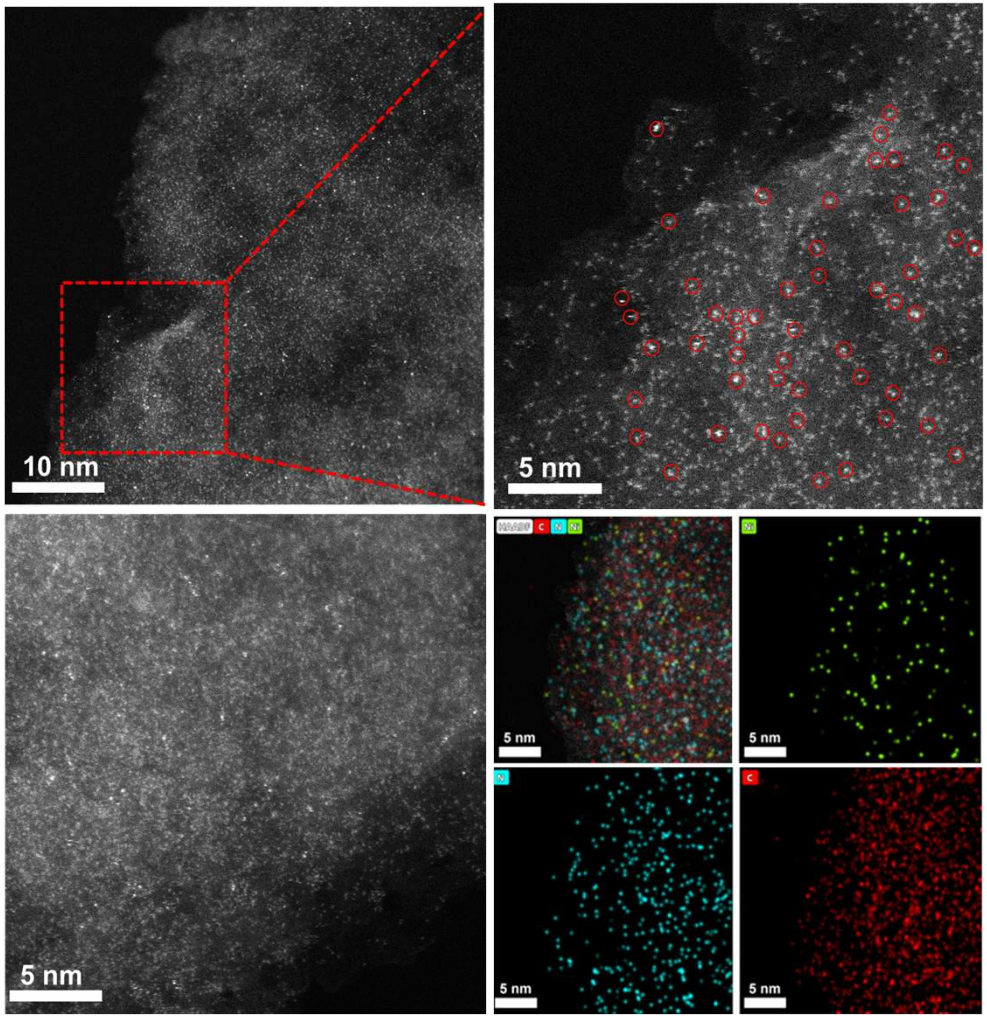

Ni/NC

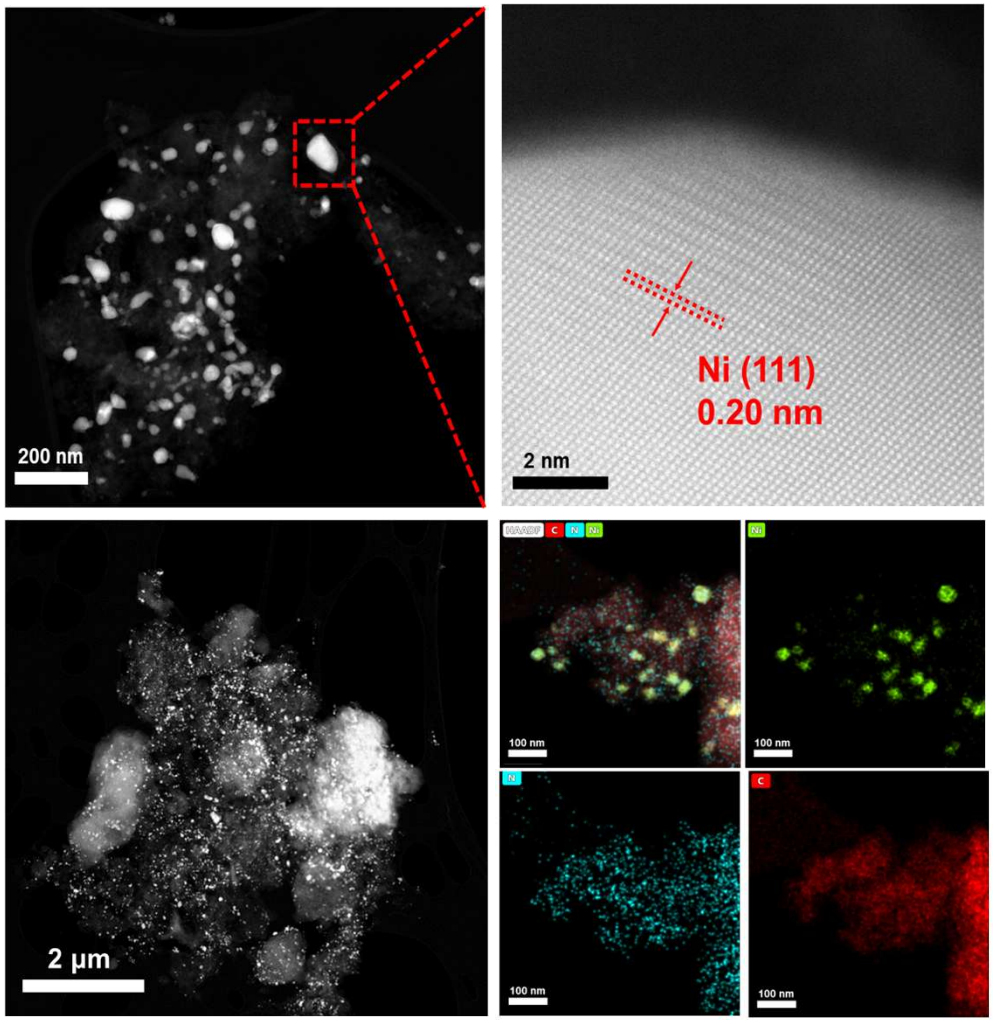

Highly dispersed SACs & Suppressing Nickel nanoparticles

Characterizations

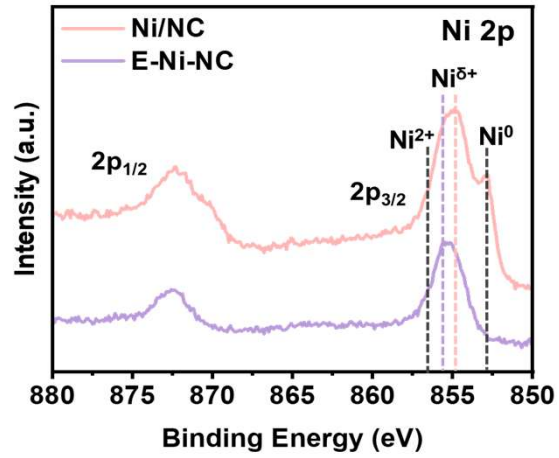

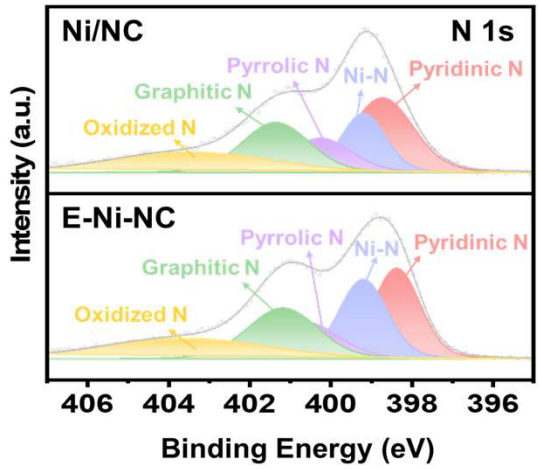

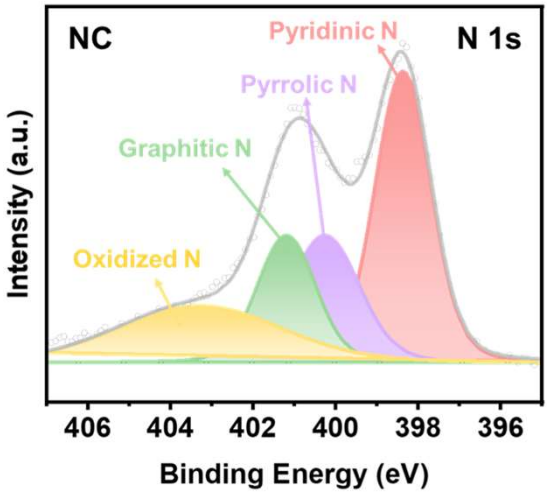

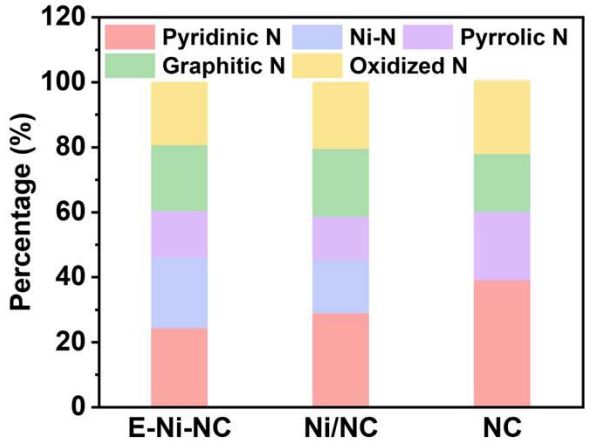

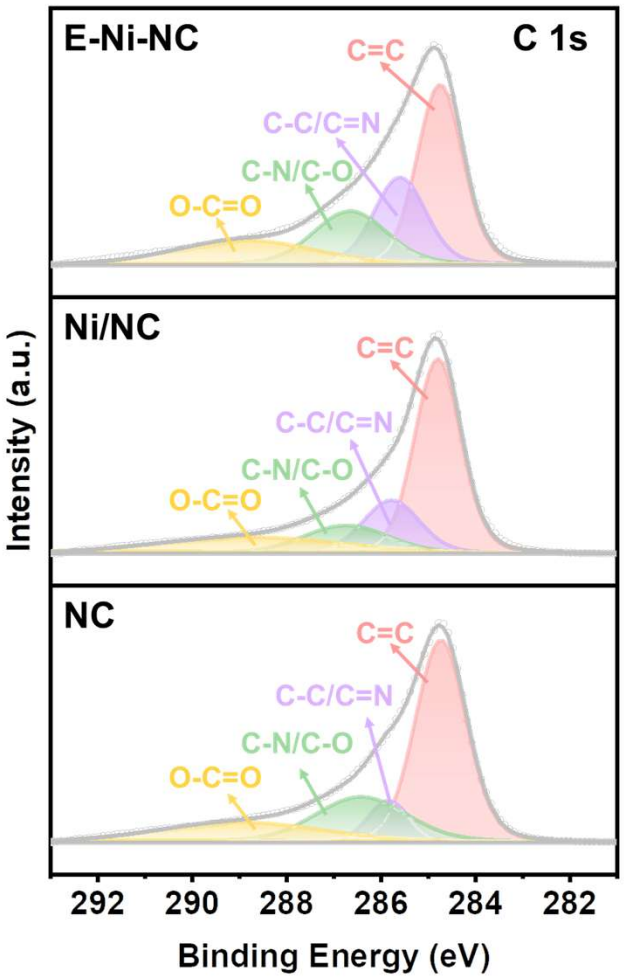

- A peak corresponding to the Ni NPs is observed in Ni 2p spectrum of Ni/NC.
- The Ni 2p$_{3/2}$ peak positions in E-Ni-NC suggest Ni valence states between 0 and +2.
- The decrease in pyridinic N content implies its potential role as anchoring sites for Ni atoms to form Ni-N sites.

Characterizations

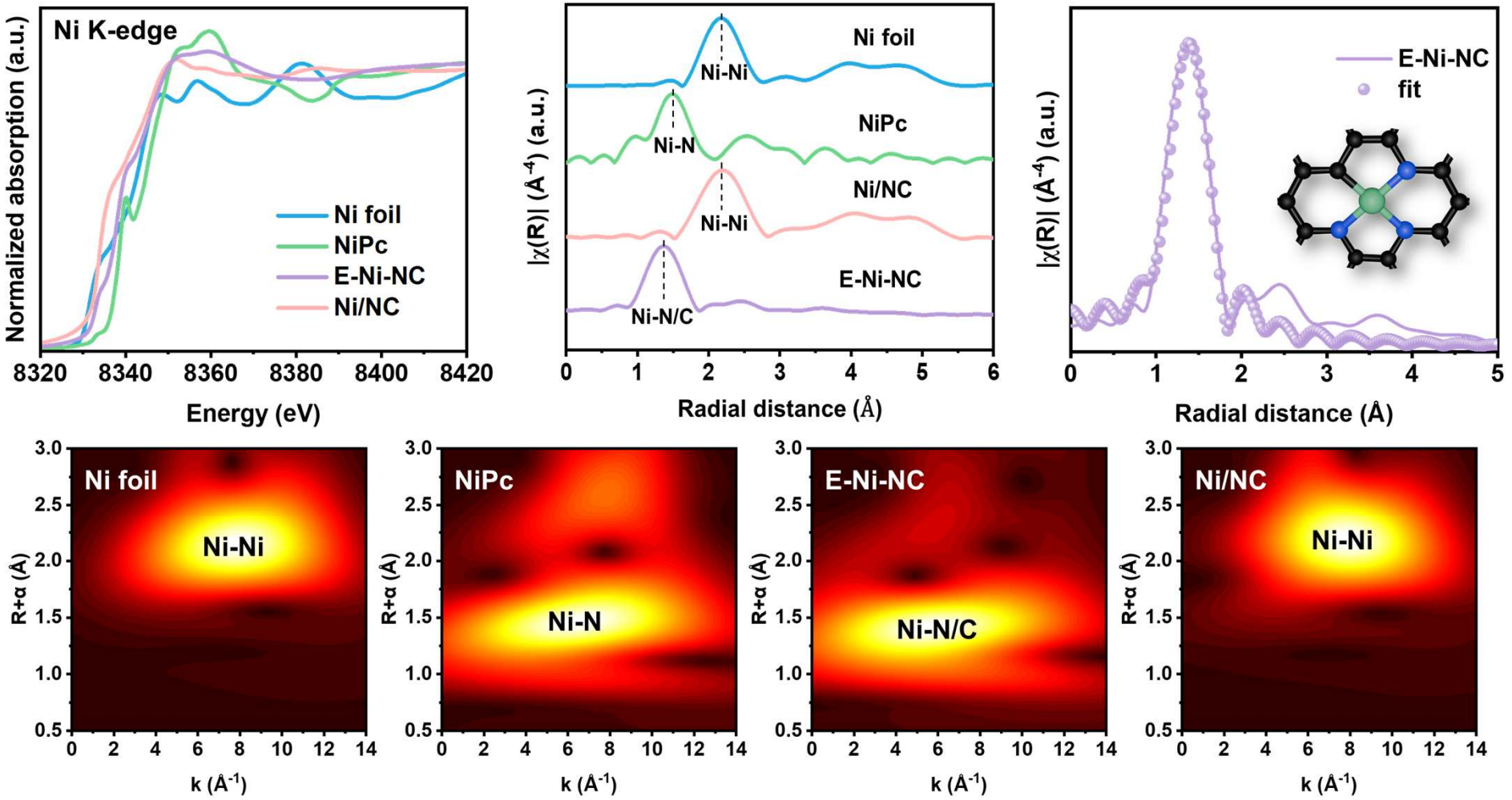

- In Ni K-edge XANES spectra, E-Ni-NC indicates a Ni valence state between 0 and +2.
- FT-EXAFS spectra of E-Ni-NC reveal a peak at ~1.38 Å, corresponding to a Ni-N/C bond.
- EXAFS fitting shows each Ni atom in E-Ni-NC is coordinated with three N and one C atoms (Ni-N_3C_1).

Electrochemical performance

➢ H-cell

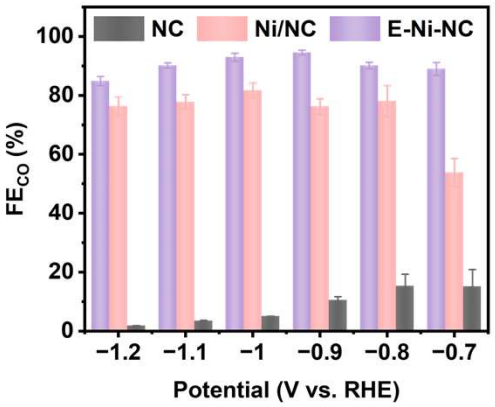

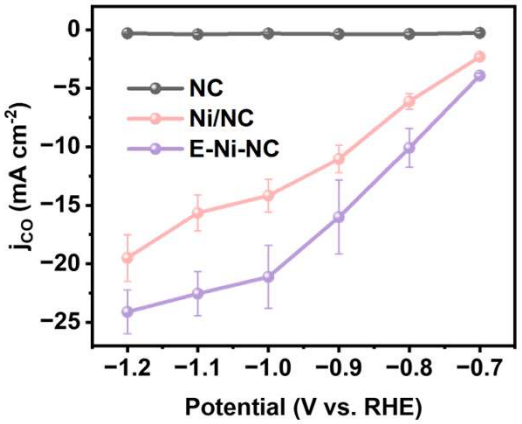

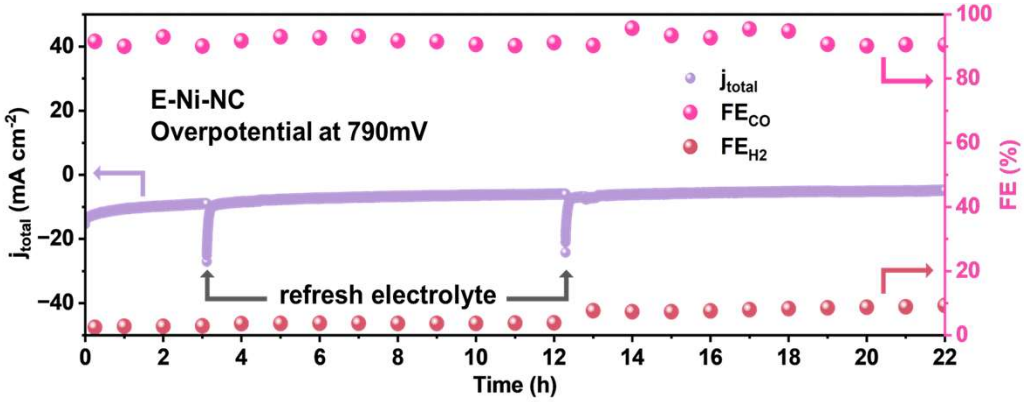

➢ Flow cell

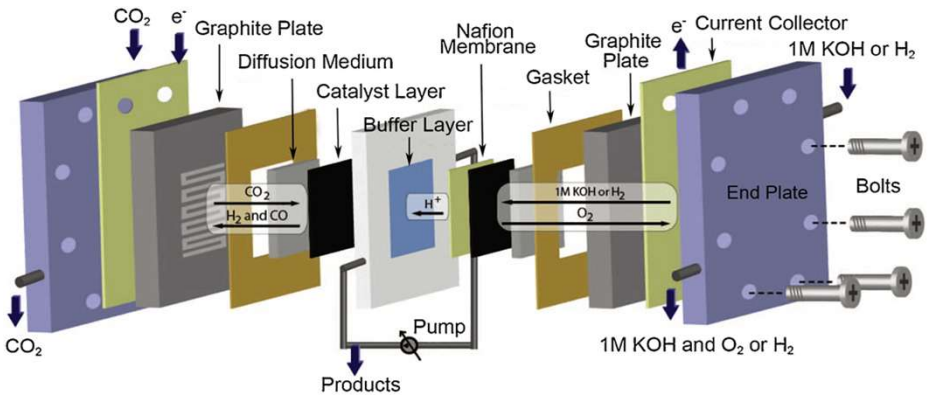

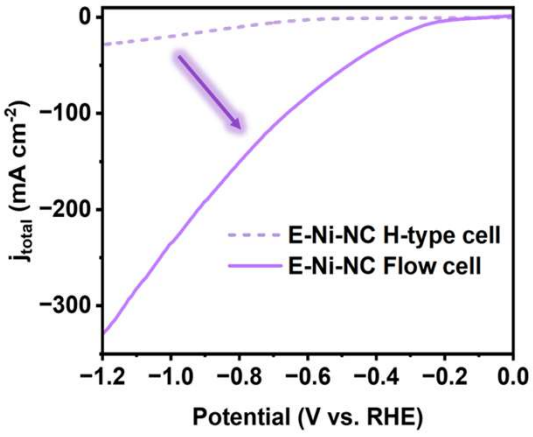

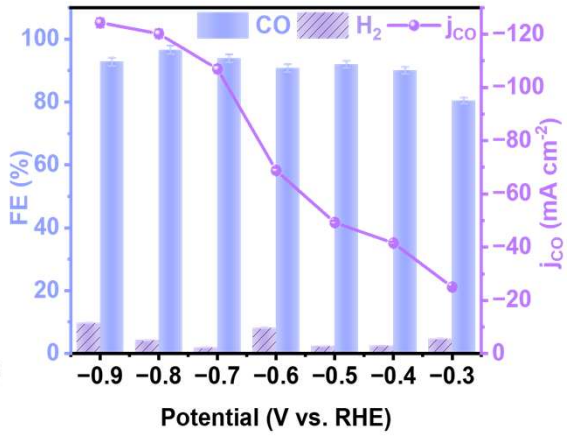

Enhanced catalytic activity & selectivity & moderate long-term stability

Theoretical Calculations

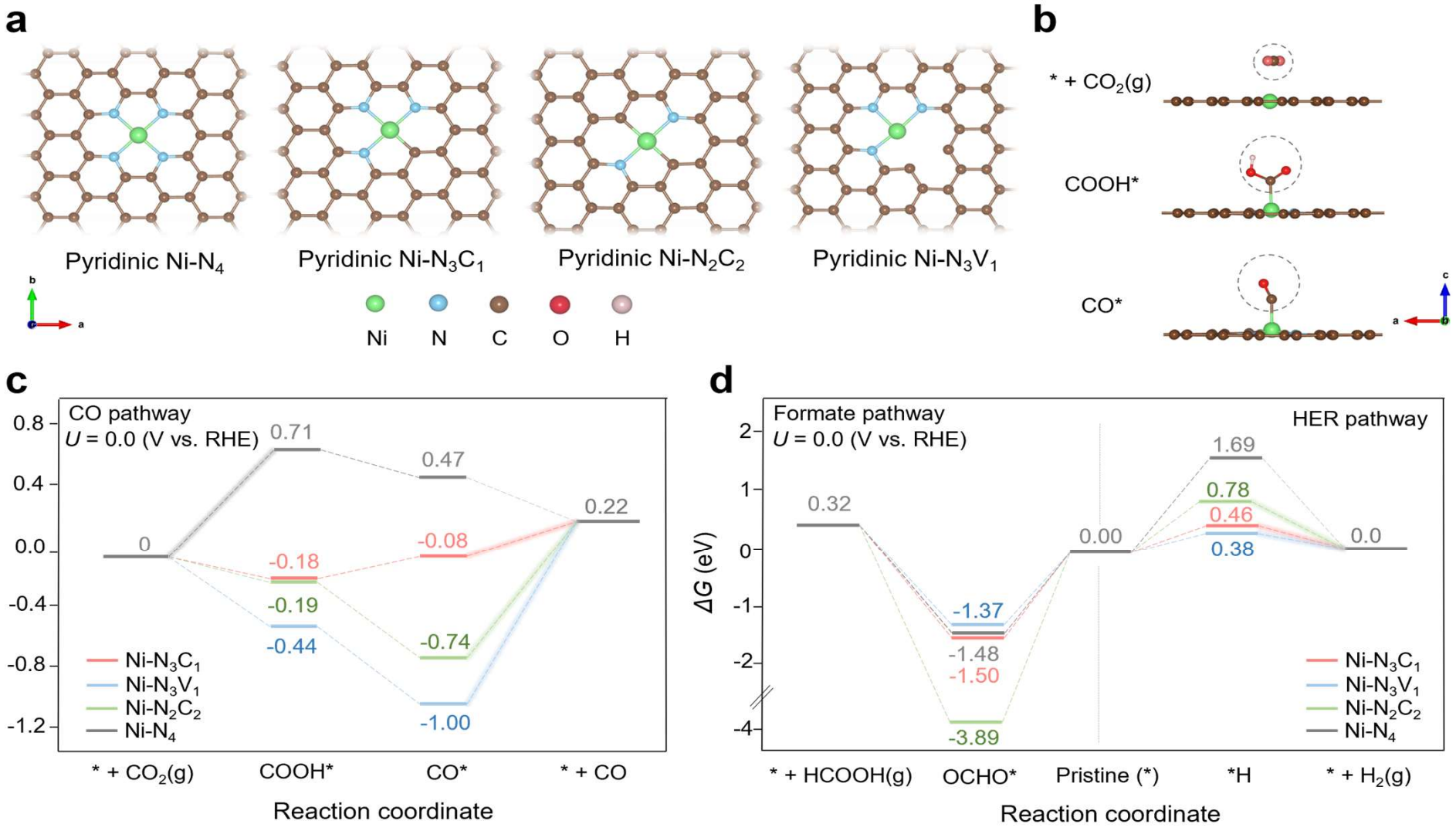

- Optimal balance between ***COOH formation & *CO desorption**

Summary

- Using **EDTA** as a strong metal-chelating ligand, we effectively **suppressed the formation of Ni NPs** and facilitated the creation of **highly dense single-atom active sites**.
- **AC-STEM** was used for structure characterization, while **XPS & XAFS** techniques were employed to analyze the chemical states and local coordination environment of the E-Ni-NC SACs.
- The E-Ni-NC SACs exhibited a high FE_{CO} value of **96.6%** and j_{CO} of **-120.2 mA cm^{-2}**, maintaining a **FE_{CO} over 90%** in a broad potential range from **-0.4 to -0.9 V** vs. RHE.
- DFT calculations further demonstrated that the asymmetric local coordination structure of **Ni-N_3C_1** within E-Ni-NC has a high ability to balance ***COOH formation and *CO desorption**, consequently enhancing the activity of E-Ni-NC for the eCO_2RR to CO.

Small vol.21, p.2409481 (2025)

Thank you for your attention